

## 4. Automotive Metals - Titanium

---

### A. Low-Cost Titanium Powder for Feedstock

---

Principal Investigator(s): Curt A. Lavender and K. Scott Weil  
Pacific Northwest National Laboratory  
P.O. Box 999, Richland, Washington 99352  
(509) 372-6770; email: curt.lavender@pnl.gov  
(509) 375-6796; email: scott.weil@pnl.gov

Industry Participants: Andrew Sherman - Ford Motor Company  
Ajit Desai - Chrysler  
Anil Sachdev - General Motors  
Vladimir Moxson - ADMA Products Inc.  
Bill Ernst - International Titanium Powder

Technology Area Development Manager: William Joost  
(202) 287-6020; email: william.joost@ee.doe.gov

Field Technical Manager: Mark T. Smith  
(509) 375-4478; email: mark.smith@pnl.gov

Contractor: Pacific Northwest National Laboratory  
Contract No.: DE-AC05-76RL01830

### Objective

---

- Enable the reduction of vehicle mass by developing low-cost titanium (Ti) feedstock materials and processing routes.
- Investigate alternate powder and melt processing methods for low-cost Ti materials.
- Evaluate processing methods to produce powder metallurgy (P/M) Ti products with International Titanium Powder, Inc. (ITP) powder.
- Evaluate the suitability of emerging Ti technologies for the production of low-cost Ti products for automotive applications.

### Approach

---

- Demonstrate integrated processing of Ti powders to produce Ti rod materials suitable for automotive spring applications.
- Perform characterization and analysis of the sintering behavior of the ITP powder. Provide feedback of results to ITP for use in process design.

- Develop low-cost feedstocks for P/M use in automotive applications.
- Survey emerging technologies for low-cost production of Ti powders and evaluate for use in automotive applications.
- Develop low-cost consolidation methods for the new Ti powders as needed to facilitate transfer to industry.

## Accomplishments

---

- *Milestone:* Demonstrate powder and in-die on high volume gear pressing (Completed October 2008).
- *Milestone:* Complete assessment of halides for alloy development and present results at Offsite Review at USCAR (Completed September 2009).
- *Milestone:* Characterize emerging Ti powders identified during FY08 cost study (Completed December 2008).
- *Milestone:* Characterize automotive prototypic component from new low-cost powders (Completed October 2009).
- Developed sintering cycles and rod-rolling conditions to produce low-cost Ti-1Al-8V-5Fe wt% (Ti185, titanium with weight percents of 1 aluminum, 8 vanadium and 5 iron) bar stock with strength levels suitable for use in automotive suspension applications. Rod stock produced exhibited yield strengths in excess of 1600 MPa far exceeding the typical yield strength requirements for steel of 1200 MPa, at 55% of the density.
- The elastic modulus for the low cost Ti185 rods was less than the 105 GPa maximum required to produce a highly mass efficient spring. The combination of strength and modulus would allow for the design of a spring from solid bar of less than 50% of the mass of an equivalent steel coil spring.
- A Ti powder containing only vanadium as a beta stabilizer produced using the ITP process was evaluated for mechanical properties demonstrating that a simple binary could stabilize the beta further lowering the cost to produce high strength low modulus beta Ti alloys.
- Developed press-and-sinter cycles that produced greater than 97% dense bars of Ti6Al4V from low-cost titanium dihydride (TiH<sub>2</sub>) powder.
- A low-cost precursor for the alloying addition of iron to the ITP process has been identified, and its use was discussed with Cristal Global, the new owner of ITP.
- A series of die and powder lubricants based on aromatic hydrocarbons was evaluated and increased green density of the ITP powder. This process was validated as it met the needs for high volume production of Ti components from ITP powder.
- The instrumented, double-acting die developed to evaluate the pressing behavior of Ti powders has been used to begin to develop a standard method for powder pressing.

## Future Direction

---

- This project in its current form will transition from Lightweighting Materials to Propulsion Materials (This report includes work funded by the Propulsion Materials activity).
- Perform fatigue testing on low-cost beta Ti bars for use in suspension applications.

- Perform fatigue testing on low-cost, processed Ti with weight percents of 6 aluminum and 4 vanadium (Ti6Al4V) bars for use in propulsion applications.
- Perform a modeling study on the effect of Ti on the fuel economy of a vehicle through substitution of materials used in propulsion applications.

## Introduction

---

This project has been a collaborative effort between Ford, General Motors, Chrysler, Pacific Northwest National Laboratory (PNNL), and the Ti raw material producers and is focused on the development and evaluation of low-cost feedstock materials produced by emerging low-cost Ti production technologies. In the next fiscal year, the project will transition to a project more focused on Ti in propulsion applications.

The purpose of this project is to develop and demonstrate materials and processing methods for producing low-cost Ti feedstock materials and automotive components. The project will evaluate and validate all processing steps necessary to produce low-cost Ti materials capable of meeting automotive property requirements.

Ti-fabricated metal products possess a combination of properties that could substantially increase the performance and reduce the mass of automobiles. Although Ti has been used in low-production volume specialty and racing automobiles, widespread use of Ti in high-volume production vehicles has been prevented by the significant expense of producing Ti components. The cost to extract Ti metal from beach sand by the conventional Kroll process alone exceeds the cost targets needed for most automotive uses. In recent years, several new processes for Ti metal production have been developed and are projected to meet the cost targets of the automotive industry. This project will survey the Ti industry for emerging technologies and evaluate their suitability as feedstock for automotive applications through technical cost studies and characterization.

Many of the newly developed processes produce Ti in a powder product ready for use in the solid state consolidation processes. Solid state Ti consolidation by powder metallurgy (P/M) methods will substantially reduce the secondary processing costs by eliminating energy-intensive and low-yielding conventional ingot processing technology. Because each new process produces a powder with unique processing requirements and there is virtually no commercial Ti P/M industry, PNNL will perform processing trials on each powder product that has been projected to satisfy automotive cost goals.

## Approach

---

The earlier phase of this project was focused on the selection of low-cost powder. The low-cost titanium dihydride powder,  $TiH_2$ , produced by ADMA Products, Inc., was selected for further evaluation. The current phase will be directed at the production of semi-finished products of automotive interest using  $TiH_2$  powder. During this reporting period, there were two demonstrations of low-cost secondary processing of Ti: 1) a low-cost beta alloy by cold isostatic press (CIP), sinter, and rod rolling, and 2) the Ti6Al4V alloy made by CIP and sintering.

## Results and Discussion

---

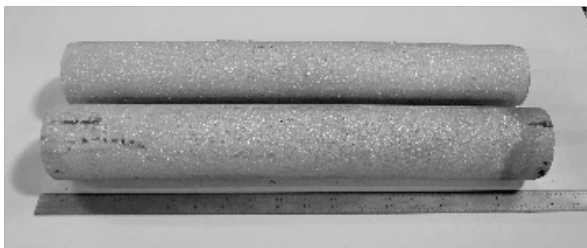
### *Development of Low-Cost Beta Ti Alloy Bar Stock*

Project work for this reporting period includes progress on the development of a low-cost, high-strength beta Ti alloy by hot rolling that will, per Dr. Andrew Sherman of Ford Motor Company, likely

be substituted for high-strength steels in applications such as fasteners, springs, valve-train, and suspension components. The mass savings associated with substitution of beta Ti for steel in such applications can be greater than 50%, and, in the case of hollow Ti used for springs, the savings can exceed 70%<sup>(2)</sup>.

The primary reason Ti has not been used for high-volume automotive applications has been cost. Typically, high-strength Ti alloys used in spring applications use up to 30% by weight Molybdenum (Mo), V and/or Chromium (Cr) to stabilize the beta phase. Therefore, the alloying constituents can cost more than the Ti metal. One low-cost alloying element able to stabilize the beta phase is iron (Fe). However, when more than approximately 2.5 weight percent of Fe is used in conventional ingot processing, the Fe tends to segregate and create inhomogeneous structures and poor fracture, ductility, and fatigue properties. If Fe could be used in higher concentration, there would be a significant cost reduction in the alloy. One method to increase the Fe content without segregation is by consolidating below the liquid phase, where buoyancy effects that results in segregation can be prevented<sup>(3)</sup>, and the Fe distribution would be controlled by solid state diffusion. In the 1950s, the Mallory Sharon Titanium Company<sup>(4)</sup> produced small heats from an alloy composed of (in weight percent) 1Al, 8V, and 5Fe called Ti185. The alloy was discontinued due to Fe segregation; however, the small heats that were solidified rapidly did produce good mechanical properties. During this reporting period, a process was developed to blend, press, sinter, and hot roll the Ti185 alloy to determine if the properties could be reproduced in a low-cost process that prevents segregation. Along with the Ti185, two additional alloys (in weight percent) 6Al and 4V and 5Al, 5V, 5Mo, and 3Cr were produced. The Ti64 alloy and Ti5553 were considered easier-to-process alloys and would be used as a baseline to compare with the Ti185 alloy.

The TiH<sub>2</sub> powder was blended and sintered into 90 mm diameter billets for rolling to 16 mm diameter rod (shown in Figure 1).



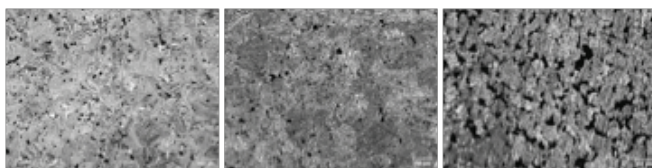
(a)



(b)

Figure 1. Typical 90 mm Ti Billets (a) Used to Hot-roll 16 mm Rods (b) from the Ti64 and Ti185 Alloys

The sintering cycle was a simple slow ramp to approximately 1350 °C, a brief hold, and furnace cooling to room temperature. At approximately 450 °C, the hydrogen began to evolve, and, by the end of the 1350 °C hold, all of the hydrogen was removed and the billets contained less than 30 ppm of hydrogen. The as-polished sintered microstructures (Figure 2) showed very high density for the Ti185 and Ti64 alloys. However, the Ti5553 (considered a easier-to-process alloy) showed significant porosity.



(a)

(b)

(c)

Figure 2. The As-sintered Microstructure Showing the Porosity (dark phase) in the Ti64 (a), Ti185 (b), and Ti5553 (c) Alloys (Notice coarse almost interconnected porosity found in the Ti5553 alloy; this alloy has been discontinued from the project.)

Densities were determined and found to be approximately 98%, approximately 98%, and 92% of theoretical for the Ti64, Ti185, and Ti5553 alloys, respectively. Etched microstructures for the billets (Figure 3) show the typical alpha+beta structure for the Ti64, a homogeneous beta structure with grain boundary alpha for the Ti185, and an apparently coarse beta structure for the Ti5553.

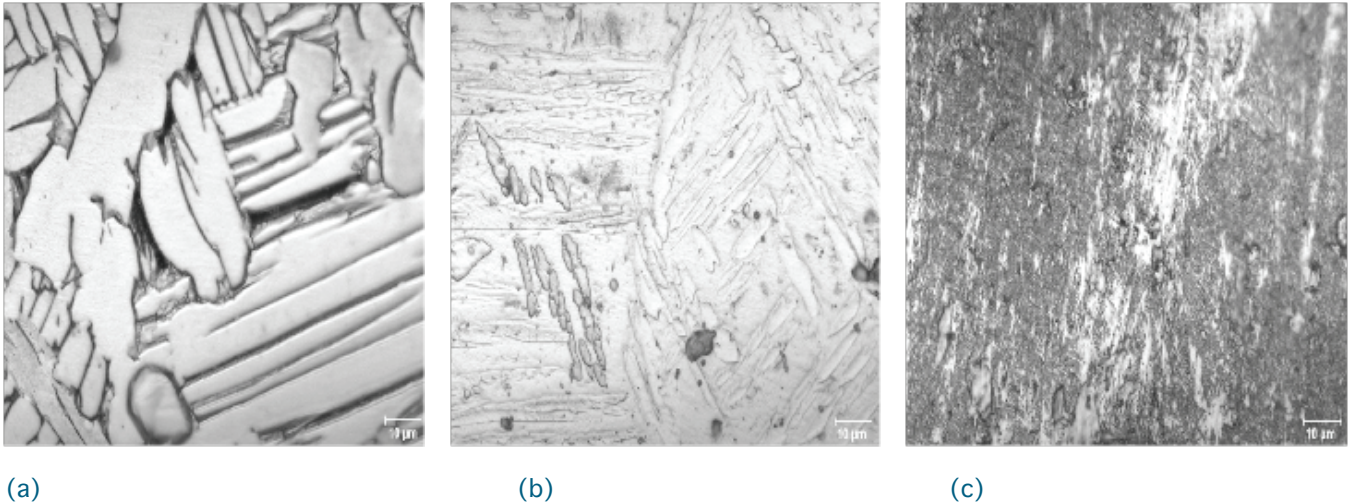


Figure 3. Optical Micrographs of the As-sintered Microstructures for the 90 mm Billets Prior to Rolling [Ti64 (a), Ti185 (b), and Ti5553 (c)].

The 90 mm billets were then rolled using a rod-mill designed for steel bar. The initial trials were quite surprising since the Ti185 alloy rolled at 800 °C produced 16 mm bars and virtually no yield loss with the billets being heated and rolled to bar in a standard steel rolling sequence, as shown in Figure 4.

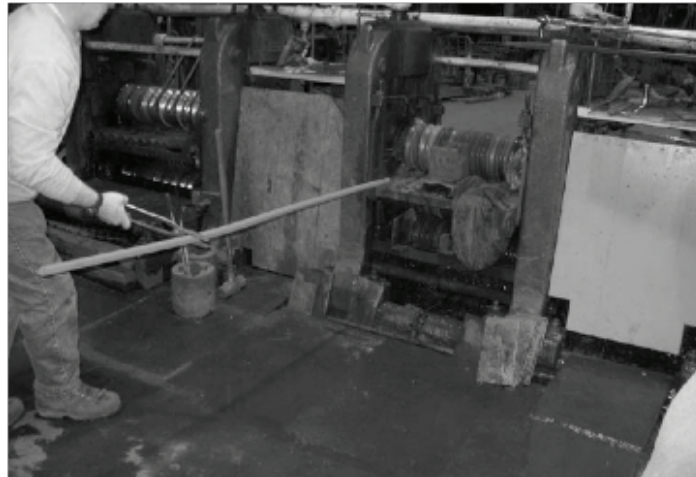


Figure 4. Hot Rolling of the Ti185 Alloy to 16 mm Rod Stock

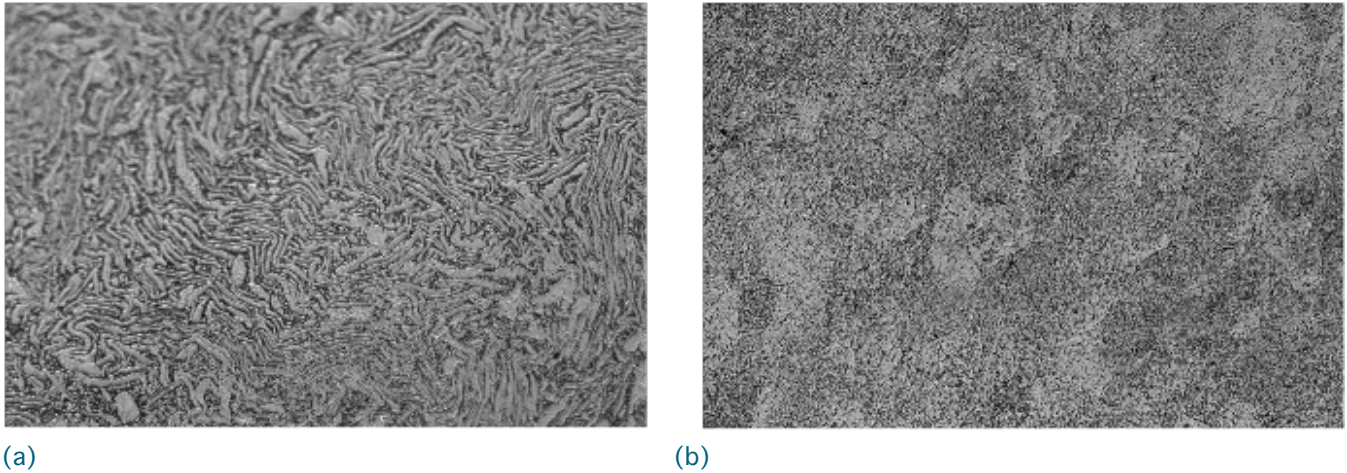
However, the Ti64 and Ti5553 alloys did not roll through initial pass without excessive cracking as shown in Figure 5.



Figure 5. Excessive Cracking Encountered in the Initial Rolling Trials of the Ti64 (top) and Ti5553 (bottom) Alloys

Billets were re-fabricated from the Ti64 and Ti5553 and a smaller initial reduction was made. The Ti64 alloy was successfully processed to 16 mm rod. The Ti5553 continued to have excessive cracking (possibly related to billet porosity) and because of the Ti185 alloy's easier processing, coupled with the high cost of the alloying constituents, work with this alloy was discontinued.

Microstructural analysis of the Ti64 and Ti185 alloy rods revealed that porosity observed in the billet was closed during the hot reduction as shown by the as-polished microstructures in [Figure 6](#). Etched microstructural analysis shows the “spaghetti” alpha+beta structure for the Ti64 and fine equiaxed beta structure with fine grain boundary alpha for the Ti185.



**Figure 6.** Optical Micrographs of the As-rolled Ti64 (a) and Ti185 (b) Alloys (The etched microstructural analysis show the “spaghetti” alpha+beta structure for the Ti64 and fine equiaxed beta structure with fine grain boundary alpha for the Ti185.)

The microstructures for both rods appear identical to the structures expected for ingot-processed materials for the given rolling conditions. Tensile test samples were removed from each rod, and the yield and ultimate strengths were 1410 MPa and 1450 MPa and 1030 MPa and 1140 MPa for Ti185 and Ti64, respectively. The as-rolled ductility for the Ti64 was 17%. It was 2% for the Ti185.

The combination of strength and ductility observed for the Ti64 was typical of that measured in wrought-processed rod stock. The unique aspect of the solid state process developed during this effort is the near 100% process yield and lack of beta forging. Using conventional ingot metallurgy processing, ingots are forged to refine the as-cast microstructure and processed to a semi-finished shape, such as a log or slab. The production of this semi-finished product from ingot usually results in a yield loss on the order of 50%. Due to the lack forging loss and the ability to direct roll, the solid state process developed here will result in a process cost savings greater than 50% over conventional ingot processing.

The Ti185 alloy typically would be heat treated to produce an optimum combination of strength and ductility. An extensive heat treatment study was performed (too lengthy to report here) and an example of the data generated can be found in [Figure 7](#), which shows an aging curve for the 750 °C solution heat treatment. The Ti185 heat treated in an optimum condition had yield and ultimate strengths of 1620 MPa and 1660 MPa, respectively, while ductility was measured at 8%. This combination of strength, ductility, and simple high-yield processing will yield a low-cost Ti alloy for use in spring applications.

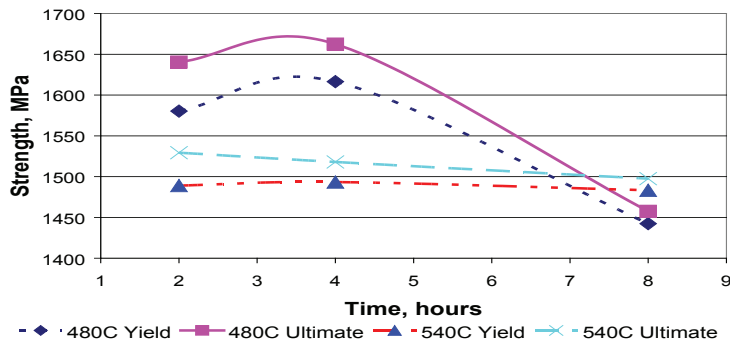


Figure 7. The Age Time Versus Strength Plot for the Ti185 Alloy Solution Treated at 750 °C and Aged at 480 °C and 540 °C.

Projections for this type of process in high volume are less than \$5/lb for heat-treated and peeled bar stock<sup>(5)</sup>. Using a simple ratio of density, the equivalent cost compared to steel would be \$2.75/lb, given the efficiency of Ti as a spring. Where 50% or less mass is required, this cost would be close to \$1.30/lb.

Unaccounted for in the simplistic analysis is the space efficiency of a Ti spring. In most examples where Ti is substituted for steel, it is directly inserted into the space occupied by the steel spring. However the equivalent Ti spring occupies less space, and additional mass savings could be accounted by compounding the mass saving associated with the adjacent components.

## CIP and Sinter

There are many components in propulsion and, potentially, automotive systems that can or could use forged Ti6Al4V. Typically, the alloy is processed from Electron Beam/Vacuum Arc Remelting (EB/VAR) ingots cogged to produce a large log that is forged and sectioned by machining to produce a blank, which then is re-forged to produce a blank for machining. In normal processing conditions, the yield loss associated with blank production can be as much as 60%. In addition to the yield loss associated with forging, Ti has high elevated temperature strength and is difficult to forge to near-net shapes. The machining loss for Ti forgings can be as high as 90%, resulting in a yield as low as 6% (the aerospace industry calls this a 17:1 buy-to-fly ratio). Of course, this yield loss is highly variable with part design and requirements. However, if equivalent mechanical properties can be produced with a near 100% yield CIP and sinter blank, the cost savings could be substantial. The yield savings alone could be as much as 60% and potentially much higher if the blank can be pressed closer to the final shape, and the machining loss is reduced.

The challenge of CIP and sinter process is matching the fatigue life of the forged Ti64. Work performed by Ivasishin<sup>(6)</sup> suggested that the Ti64 alloy processed from TiH<sub>2</sub> powder, which sinters readily to high density, may meet the requirements for fatigue. However, Ivasishin die-pressed at high pressure. Therefore, the purpose of this task is to examine if a large part, i.e., 150 mm in diameter, can be CIP pressed and sintered and demonstrate sufficient fatigue life.

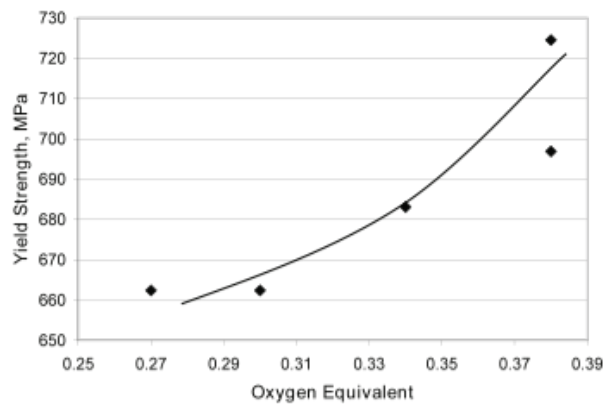
The CIP and sinter effort has been initiated, with initial trials focused on determining the levels of Fe and O that must be added to the powder to produce 725 MPa yield strength in the annealed condition. Normally, specifications for the Ti64 require the alloy to exhibit a minimum yield strength of 725 MPa (or higher in some cases) when fully annealed. This is accomplished by adding Fe and O to the alloy to develop interstitial strengthening. When CIP pressed and sintered, the Ti64 produced from the TiH<sub>2</sub> has a yield strength of approximately 550 MPa without Fe or O additions. Therefore, a series of four compositions with variable Fe and O and the as-received powder were CIP pressed and sintered from the TiH<sub>2</sub> powder in cylinders

approximately 90 mm in diameter (the actual compositions are provided in Table 1). The alloys were labeled 0 to 4, where 0 was the as-received consolidated powder and 1 through 4 were varying levels of Fe and O below the normal specification limits.

Table 1. Fe and O Trial Results

Alloy	Element				Oxygen-equivalent	Yield Strength MPa
	C	O	N	Fe		
0	0.001	0.192	0.022	0.083	0.27	662
1	0.009	0.289	0.021	0.130	0.38	697
2	0.009	0.176	0.022	0.320	0.30	662
3	0.010	0.227	0.024	0.200	0.34	683
4	0.010	0.249	0.023	0.340	0.38	725

The alloys 1 and 2 had the highest yield. However, only alloy 4 approached and barely met the minimum yield strength required. The yield strength should correlate to the “oxygen” equivalent (Equation 1), where the three main interstitial strengthening elements O, C, and N are combined with Fe. Alloys 1 and 4, which had the highest oxygen equivalent also had the highest yield strengths. Alloy 2 had the lowest oxygen equivalent alloys and, with the as-received powder alloy 0, had the lowest strength. Further confirmation of the oxygen-equivalent trend can be seen in Figure 8 plot that shows the upward trend for yield strength and oxygen equivalent.



$$\text{Oxygen Equivalent} = \text{O} + 2.77\text{N} + 0.2\text{C} + 0.2\text{Fe} \quad (1)$$

Figure 8. Yield Strength as Function of Oxygen Equivalent for Ti64 Test Alloys Used in the CIP and Sinter Development Activity

Ideally, the strengths would be higher, providing a greater margin for design. Upon examination of the microstructures (see Figure 9), it showed a higher level of porosity than desired, which may be influencing the decreased strength level. This porosity is very fine with pore sizes of less than 20 μm and not interconnected a likely result of incomplete compaction and sintering. Because the porosity is not interconnected and, thereby, not surface-connected, the bars can be hot-isostatic pressed (HIP) to heal the porosity, which should yield an increase in tensile strengths. HIP trials are underway to close the porosity. Once the strength levels are achieved, samples will be submitted for fatigue testing.

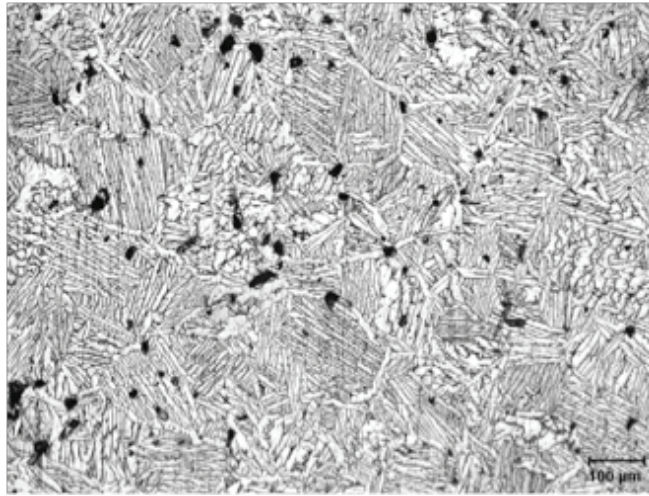


Figure 9. The Porosity Observed in the Ti64 Test Alloys Used in the CIP Development Activity

## Conclusions

---

The conclusions reached during this reporting period are as follows:

- A beta Ti alloy, Ti1Al8V5Fe, was produced using a low-cost  $\text{TiH}_2$  powder featuring low-cost Fe constituent as the primary beta stabilizer.
- Solid state consolidation and hot rod rolling of a high-strength beta alloy made from a low-cost  $\text{TiH}_2$  powder was demonstrated and produced rods with near 100% yield from incoming powder. After solution heat treatment and age, the alloy exhibited yield and ultimate strengths of 1620 MPa and 1660 MPa, respectively, with 8% elongation.
- A beta titanium alloy, such as Ti185, could replace high-strength steel in many automotive applications, such as fasteners and valve strain components. When a high-strength beta alloy is substituted for steel in spring applications, the mass savings can exceed 50%.
- Progress was made on the development of a low-cost Ti64 by CIP and sinter for the replacement of forgings. If the Ti64 could be produced with a sufficient cost reduction, a series of engine components currently made from aluminum can be replaced, allowing for higher operating temperatures and better engine efficiency.

## References

---

- Lavender CA, et al. 2009. "Low Cost Titanium for Feedstock" October 2009, USCAR LAMETS 2009.
- Zagrebelnyy D and MJM Krane. 2009. "Segregation Development in Multiple Melt Vacuum Arc Remelting." Metallurgical and Materials Transactions B40(3):281-288.
- Abkowitz, S. 1957. Engineering Test Report. Mallory-Sharon Titanium Company, Niles, Ohio.
- Moxson V. 2009. "Low Cost Titanium using  $\text{TiH}_2$ ." International Titanium Association Annual Meeting.
- Ivasishin O, et al. 2006. "Synthesis of Powder Metallurgy Titanium Using Hydrogenated Titanium." May 15-18, 2006, Seattle, Washington. 17th AeroMat Conference & Exposition.

## B. Production of Heavy Vehicle Components from Low-Cost Titanium Powder

---

Principal Investigator: Seong Jin Park  
Associate Research Professor  
Center for Advanced Vehicular Systems, CAVS, 2215  
Mississippi State University, P.O. Box 5405  
Mississippi State, MS 39762-5405  
(662)325-8565; e-mail: sjpark@cavs.msstate.edu

Co-Principal Investigator: Antonyraj Arockiasamy  
Center for Advanced Vehicular Systems  
Mississippi State University, P.O. Box 5405  
Mississippi State, MS 39762-5405  
(662)325-8558; e-mail: aanton@cavs.msstate.edu

Co-Principal Investigator: Haitham El Kadiri  
Assistant Research Professor  
Center for Advanced Vehicular Systems  
Mississippi State University, P.O. Box 5405  
Mississippi State, MS 39762-5405  
(662)325-5568; e-mail: elkadiri@cavs.msstate.edu

Co-Principal Investigator: Youssef Hammi  
Center for Advanced Vehicular Systems  
Mississippi State University, P.O. Box 5405  
Mississippi State, MS 39762-5405  
(662)325-5452; e-mail: yhammi@cavs.msstate.edu

Technology Area Development Manager: William Joost  
(202) 287-6020; e-mail: william.joost@ee.doe.gov

Contractor: Mississippi State University  
Contract No.: DE-FC-26-06NT42755

### Objective

---

Design and produce titanium (Ti) structural components by using math-based, experimental-validated powder compaction and sinter models.

### Approach

---

Examine low cost blended elemental (BE) and prealloyed (PA) Ti powders that are responsive to the powder metallurgy process and synthesize new combinations and innovations in the powders' compositions. Recent developments, such as using hydride powders, have enabled the fabrication of BE parts to over 99% of full density, resulting in significantly improved properties. Additives such as carbon or boron can then generate carbide or boride reinforcing phases – dispersed phase composites. Further studies and developments have shown that this approach may be well suited in reducing the cost in automotive parts production, thus making Ti more cost competitive with other materials commonly used. This work will include powder modifications, novel organo-metallic lubricants (the composition is proprietary), finite element analysis of the

compaction to minimize wall friction and wear, and the evaluation of novel tooling materials and coatings. New computer tools for modeling porosity and size change during both compaction and sintering will be tailored to Ti systems, giving them the ability to perform computer aided design for the tooling and the processes to attain dense and net-shaped final products.

## Accomplishments

---

- Literature survey for low cost Ti powder, Ti alloys for automotive application with cost analysis, and their processing techniques.
- Designed new Ti alloys and proposed three Ti alloy candidates.
- Evaluated and selected Ti alloys, including Ti alloys containing boride based on mechanical properties, liquid phase sinterability, and cost-effectiveness.
- Performed powder injection molding (PIM) experiment.
- Simulation tool development for PIM, die compaction, and sintering with some optimization.

## Introduction

---

Lower cost Ti could be the catalyst for Ti to break into the automotive industry. The goal is to have a competitively priced Ti component produced by cost-competitive manufacturing methods. The proposed research on Ti and Ti matrix composites is the first stage in a sequence of P/M efforts geared to infuse net-shape production of lightweight materials into the domestic automotive industry. P/M techniques afford designers the ability to produce significantly complex near-net shape parts at potentially significant cost savings, with very little wasted material. [Table 1](#) shows the overall structure of Task 1 with ORNL collaboration.

**Table 1.** Overall structure of Task 1

	experiment	simulation
die compaction	ORNL	MsSt
PIM	MsSt	MsSt
sintering	ORNL	MsSt
HIPing	ORNL	MsSt

## Work Scheduled

---

[Table 2](#) shows the work accomplished based on the schedule planned. Subtasks related to the experiment were at risk in the beginning, because we needed experimental data for die compaction, sintering, and HIPing for modeling. As for the PIM, we completed the final stage of PIM experiment with help of the Pennsylvania State University.

Table 2. The proposed schedule of Task 1 with the marks of progress

Subtasks	Year 1				Year 2			
	Q1	Q2	Q3	Q4	Q1	Q2	Q3	Q4
1.1 literature review, first simulation	100							
1.2 powder evaluations	100							
1.3 microstructure and interfacial study	100							
1.4 processing evaluation	100							
1.5 modeling and simulation		100						
1.6 optimization		100						
1.7 experimental verification		100						
1.8 mechanical properties					100			
1.9 process verification						100		

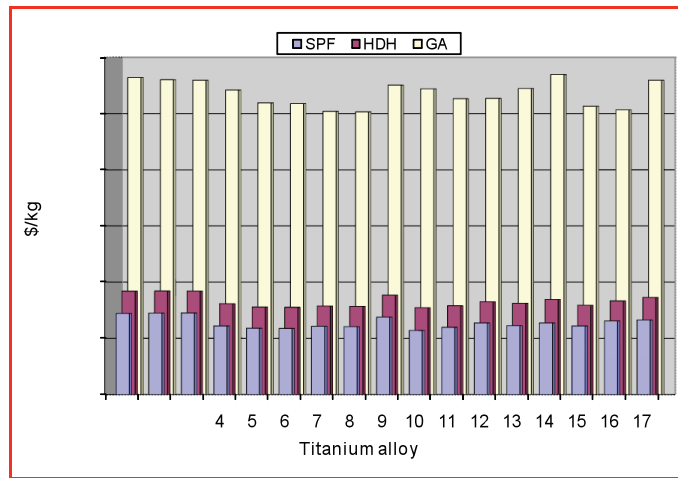
## Literature Survey

We surveyed literature for Ti powder production methods for gas atomized, HDH, sponge Ti powders, Ti alloys, P/M processes, and previous uses of Ti alloys for automotive application. The cost of Ti alloys is at least 10 times higher than the cost of Al alloys and 30 times higher than the cost of steels [1]. Table 3 summarizes the consumption of Ti alloys in the automotive market between 1998 and 2002. We have seen that Ti alloys were never used in massive production mode. They were limited only to components requiring extra high stiffness and superior maximum specific strength comparable to Al, Mg, and steels. However, manufacturers have shown a desire to use slightly more expensive Ti alloys than Al in powertrain if rotating and oscillating masses are to be substantially reduced.

Table 3. Uses of Ti alloys automotive application

year	component	material	manufacturer
1998	brake guide pins	Grade 2	Mercedes
1998	sealing washers	Grade 1s	Volkswagen
1998	gear shift knob	Grad1	Honda
1999	connecting rods	Ti-6Al-4V	Porsche
1999	valves	Ti-6Al-4V	Toyota
1999	turbocharger rotor	Ti-6Al-4V	Mercedes
2000	suspension spring	LCB	Volkswagen
2000	valve cups	b-Ti alloy	Mitsubishi
2000	turbocharger rotor	g-TiAl	Mitsubishi
2001	exhaust system	Grade 2	GM
2002	valves	Ti-6Al-4V	Nissan

We also analyzed the cost for the candidate Ti alloys, as shown in Figure 1. This analysis showed that the Ti powder type is most important factor in cost among gas atomized, HDH, and sponge Ti powders.



- |  |                                  |
|--|----------------------------------|
| 1. Ti-6Al-4V                           | 10. Ti-6Al-1.7Fe-.1Si            |
| 2. Ti-6Al-4V-1Mo                       | 11. Ti-4.5Fe-6.8Mo-1.5Al         |
| 3. Ti-6Al-4V-0.2B                      | 12. Ti-1.5Fe-6.8Mo-4.8Al-1.2Nb   |
| 4. Ti-8Al-1V-1Mo                       | 13. Ti-1Fe-1Mo-6.3Al-1.2Nb       |
| 5. Ti-6Al-2Sn-4Zr-2Mo                  | 14. Ti-1.5Fe-2.25Mo-1.2Nb-.3Al   |
| 6. Ti-6Al2Sn-4Zr-2Mo-0.2Si             | 15. Ti-6Al-4Sn-4Zr-1Nb-1Mo-.2Si  |
| 7. Ti-6.5Al-4.6Sn-4.6Zr-1Nb-.3Si-1Mo   | 16. Ti-4.3Fe-7Mo-1.4Al-1.4V-5.4B |
| 8. Ti-6.6Al-4.6Sn-4.6Zr-.9Nb-1Mo-.35Si | 17. Ti-2Co-2.Mo-1.4Al-1.4V-1.8B  |
| 9. Ti-4.5Al-3V-2Fe-2Mo                 |                                  |

Figure 1. Cost analysis plot for candidate Ti alloys.

## Ti Alloys Design

Ti alloys can be a predominant monophase structure,  $\alpha$  (hcp) or  $\beta$  (bcc) or a dual phase structure  $\alpha+\beta$ , depending on the composition strength ratio between the  $\alpha$  stabilizing elements and  $\beta$  stabilizing elements. Figure 2 schematically illustrates the main properties of potential Ti alloys, which fall into different crystallographic classes. Alpha alloys enclose only traces of betaphase. Near-alpha alloy contained predominantly alpha, and the microstructure may appear similar to an alpha alloy. A dual phase alpha-beta alloy consists of alpha and retained or partially transformed beta. Metastable beta alloys predominantly retained beta, which is susceptible to a fine transformation upon post-heat treatments. All of these alloys are used for temperatures less than 600°C, although the melting temperature is higher than that of typical steel. A thermal expansion coefficient is less than half of aluminum.

Based on our research, we recommended choosing the following three compositions using master alloy powder for generating the eutectic systems:

Ti-(2 to 3%)Fe- (3% to 6%)Zr- (2% to 4%)Sn- (1% to 3%)Mo- (0% to 1%Cr),  
 Ti-(2 to 3%)Fe- (3% to 6%)Zr- (2% to 4%)Sn- (2% to 3%)Mn- (1 to 2%)Mo- (0% to 1%Cr),  
 Ti-(2 to 3%)Fe- (3% to 6%)Zr- (2% to 4%)Sn- (2% to 3%)Mn- (1 to 2%)Mo- (2% to 5%)Cr<sub>3</sub>C<sub>2</sub>.

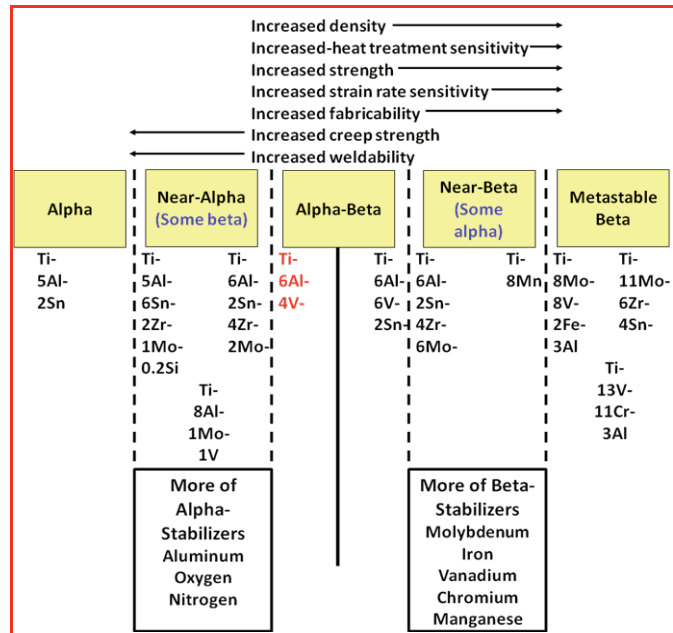


Figure 2. General classification of Ti alloys with respect to properties and microstructure.

We purchased these powders for evaluating the proposed Ti alloy compositions. The evaluation was performed through powder mixing, die compaction, sintering, and mechanical property measurement. Figure 3 shows the optimization algorithm for liquid phase sintering of Ti alloy powder.

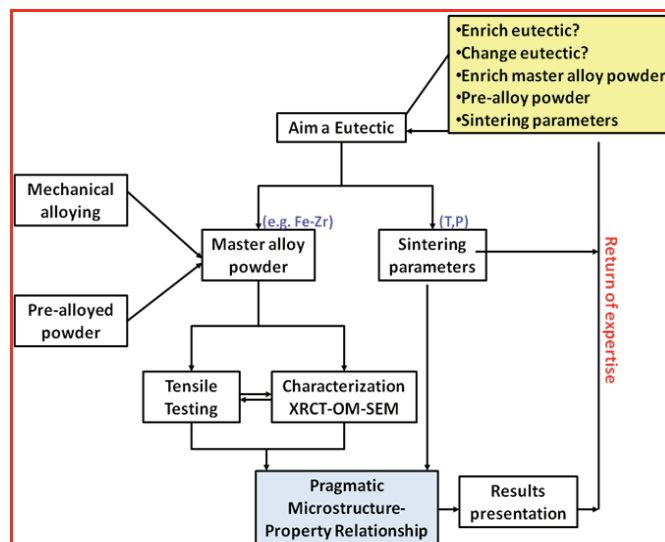


Figure 3. Composition optimization algorithm for liquid phase sintering of Ti alloy powder.

As for PIM, we prepared PIM feedstock based on the standard wax-polymer binder system with 50% solid loading percentage. We measured the viscosity using a homemade capillary rheometer to obtain the material properties for the simulations.

## Ti Alloy Simulation: ThermCal

The thermodynamic equilibrium calculations were performed using the software Thermo-Calc, Version R (Thermo-Calc Software, Stockholm, Sweden). Figure 4 shows the calculated Ti-Fe-Zr ternary phase diagram at the sintering temperature of 1275 °C. Liquid phase and other solid phases including BCC, Laves, FeTi, and Fe<sub>23</sub>Zr<sub>6</sub> were obtained. In the present study, the compositions were adjusted as 0-10 wt% Fe and 0-5 wt % Zr, where only bcc phase was obtained in the ternary system at the sintering temperature of 1275°C.

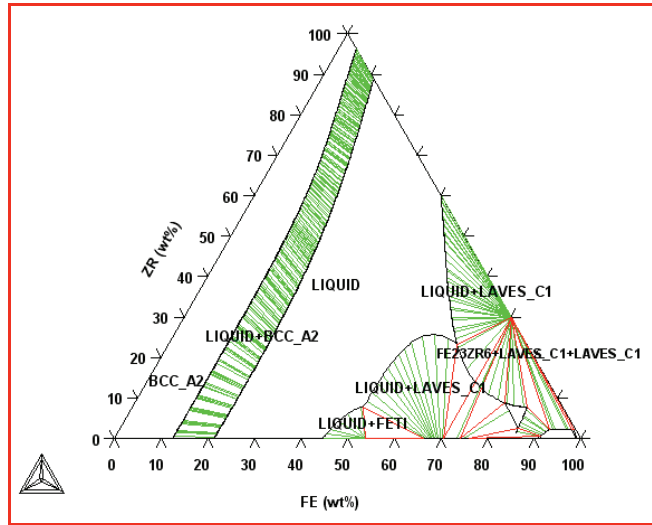


Figure 4. Ti-Fe-Zr ternary phase diagram calculated by Thermo-Calc at the sintering temperature of 1275°C.

The equilibrium phase calculations were performed at the sintering temperature of 1523 K for the compositions suggested in the previous section. For each case, three values were chosen for each composition: low, middle, and high values of the selected compositions. The mass percentage of each phase was calculated for each composition, as shown in Table 4. It can be seen that bcc phase is dominant at the sintering temperature; fcc phase may appear when carbon is added. It is noted that no liquid phase was obtained for these compositions at the current sintering temperature.

Table 4. Equilibrium phase distribution for different Ti alloy compositions at the sintering temperature of 1275°C (wt%)

No.	Ti	Fe	Mo	Zr	Sn	Cr	Mn	Cr <sub>2</sub> C <sub>3</sub>	BCC	FCC
Alloy 1	94.0	1	1	2	1	1			100	
	88.0	2	2	4	2.5	1.5			100	
	82.0	3	3	6	4	2			100	
Alloy 2	93.0	1	1	2	1	1	1		100	
	86.0	2	2	4	2.5	1.5	2		100	
	79.0	3	3	6	4	2	3		100	
Alloy 3	92.0	1	1	2	1		1	1	98.7	1.3
	83.0	2	2	4	2.5		2	3	93.9	6.1
	74.0	3	3	6	4		3	5	89.5	10.5

## Experimental Evaluation of Designed Ti Alloys

In this research, three different Ti powders were used, as shown in Figure 5: (1) sponge (DuPont), (2) hydride-dehydride (HDH; Phelly Materials), and (3) gas-atomized powders (Sumitomo Corporation). To evaluate the designed Ti alloys described in the previous section, we also purchased additive elements such as Fe, Mo, Zr, Sn, Mn, Cr, and  $\text{Cr}_2\text{C}_3$ .

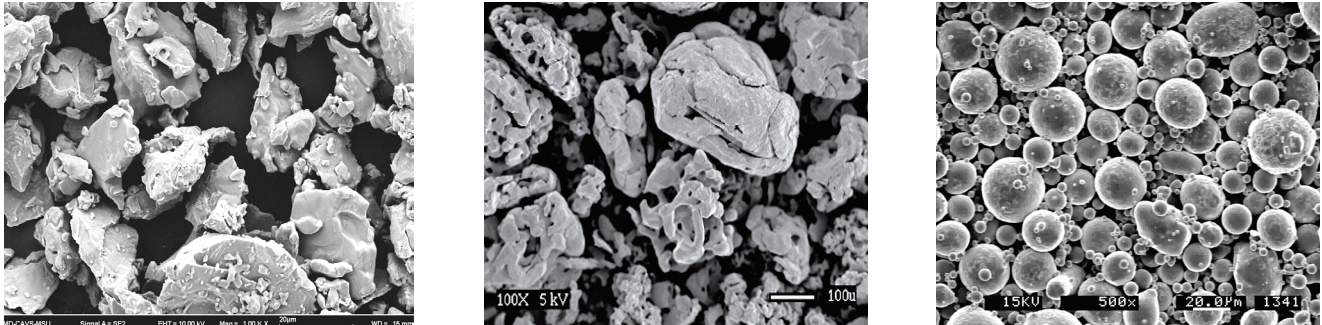


Figure 5. SEM images for three Ti powders used in this research: a) Cp Ti(-325 mesh), b) Sponge Ti (-100 mesh), and c) Cp Ti (-250 mesh).

We evaluated fifteen Ti alloys, as shown in Table 5, and selected six Ti alloys according to the following criteria in the following order:

1. Higher sintered density using liquid phase sintering (LPS) cycle,
2. Clear endothermic peak for LPS (See Figure 6.),
3. Cost of Ti alloys.

Table 5. Ti alloys evaluated and selected

ID.No		Ti	Fe	Mo	Zr	Sn	Mn	Cr	$\text{Cr}_2\text{C}_3$
1		97.0	1.5	1.5					
2		94.0	3.0	3.0					
<b>3</b>	<b>Selected</b>	<b>94.5</b>	<b>1.5</b>	<b>1.5</b>	<b>2.5</b>				
4		89.0	3.0	3.0	5.0				
<b>5</b>	<b>Selected</b>	<b>93.0</b>	<b>1.5</b>	<b>1.5</b>	<b>2.5</b>	<b>1.5</b>			
6		86.0	3.0	3.0	5.0	3.0			
7		91.5	1.5	1.5	2.5	1.5	1.5		
<b>8</b>	<b>Selected</b>	<b>83.0</b>	<b>3.0</b>	<b>3.0</b>	<b>5.0</b>	<b>3.0</b>	<b>3.0</b>		
9		90.5	1.5	1.5	2.5	1.5	1.5	1.0	
<b>10</b>	<b>Selected</b>	<b>81.0</b>	<b>3.0</b>	<b>3.0</b>	<b>5.0</b>	<b>3.0</b>	<b>3.0</b>	<b>2.0</b>	
<b>11</b>	<b>Selected</b>	<b>89.5</b>	<b>1.5</b>	<b>1.5</b>	<b>2.5</b>	<b>1.5</b>	<b>1.5</b>	<b>1.0</b>	<b>1.0</b>
12		79.0	3.0	3.0	5.0	3.0	3.0	2.0	2.0
<b>13</b>	<b>Selected</b>	<b>83.0</b>	<b>3.0</b>	<b>3.0</b>	<b>6.0</b>	<b>4.0</b>		<b>1.0</b>	
14		81.0	3.0	3.0	6.0	4.0	3.0	1.0	
15		76.0	3.0	3.0	6.0	4.0	3.0		5.0

Based on the selected six Ti alloys, we proposed sixteen Ti alloys with more combinations of additive element. We measured the mechanical properties of sixteen Ti alloys, including sintered density, hardness, ultimate tensile strength (UTS), and elongation, as shown in Table 6. Finally, we selected Ti-Fe-Zr combinations as a candidate Ti alloy.

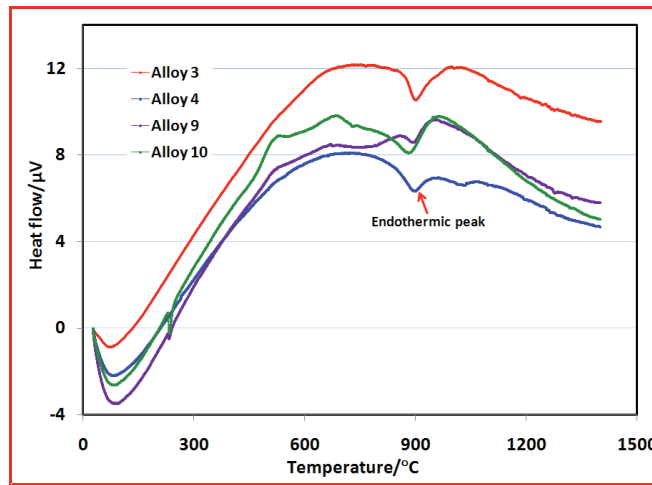


Figure 6. DSC experiment for LPS evaluation.

Table 6. Mechanical properties of selected Ti alloys.

Alloy	$\rho_{th}$ (g cm <sup>-3</sup> )	Green samples		Sintered samples (1275 °C, 60 min, 10 mtorr)				
		$\rho_g$ (g cm <sup>-3</sup> )	Relative density (%)	$\rho_s$ (g cm <sup>-3</sup> )	Relative density (%)	Hardness (HRB)	Elongation (%)	UTS (MPa)
Pure Ti	4.51	3.24	71.8	4.14	91.8	88.1	3.13	643
Ti-5Fe-2.5Zr	4.64	3.26	70.2	4.41	94.9	103.9	3.54	1025
Ti-5Fe-5Zr	4.68	3.29	70.3	4.40	94.0	104.3	2.50	1227
Ti-10Fe-2.5Zr	4.75	3.21	67.6	4.54	95.6	108.1	0.60	611
Ti-10Fe-5Zr	4.79	3.43	71.6	4.77	99.6	112.9	0.00	281
Ti-5Fe	4.61	3.39	73.6	4.30	93.3	101.7		
Ti-10Fe	4.71	3.26	69.2	4.40	93.4	104.5		
Ti-10Fe-2.5Zr-1Cr	4.77	3.21	67.3	4.37	91.7	102.6		
Ti-10Fe-5Zr-1Cr	4.81	3.34	69.5	4.43	92.2	104.4		
Ti-10Fe-2.5Zr-1.5Mo	4.79	3.44	71.8	4.59	95.8	104.8		
Ti-10Fe-2.5Zr-3Mo	4.83	3.41	70.5	4.45	92.0	105.4		
Ti-10Fe-2.5Zr-2Sn	4.79	3.31	69.1	4.44	92.7	104.1		
Ti-10Fe-2.5Zr-4Sn	4.83	3.55	73.5	4.46	92.4	103.4		
Ti-10Fe-2.5Zr-2Cr <sub>2</sub> C <sub>3</sub>	4.78	3.16	66.1	4.38	91.6	105.2		
Ti-10Fe-2.5Zr-4Cr <sub>2</sub> C <sub>3</sub>	4.81	3.28	68.1	4.53	94.1	108.3	1.40	373
Ti-10Fe-2.5Zr-1Mn	4.78	3.19	66.7	4.32	90.4	101.4		
Ti-10Fe-2.5Zr-3Mn	4.81	3.19	66.3	4.37	90.9	103.7		

We focused on the investigation of Ti-Fe-Zr alloys with microstructure analysis produced by the press and the sinter process. Samples were produced by the mixing of initial pure metallic powders followed by uniaxial pressing with subsequent densification by sintering at 1275 °C in vacuum. Scanning electron microscopy (SEM) and optical microscopy (OM) were used to study the microstructure of the sintered samples. Figure 7 shows the importance of vacuum level in Ti alloy sintering. Hardness and tensile tests were performed for each sample. The results show that as Fe and Zr increase, the theoretical density and the mechanical properties increase, as listed in Table 7. The maximum properties of samples were obtained with the addition of 5Fe-5Zr wt% at 1275 °C for 60 min.

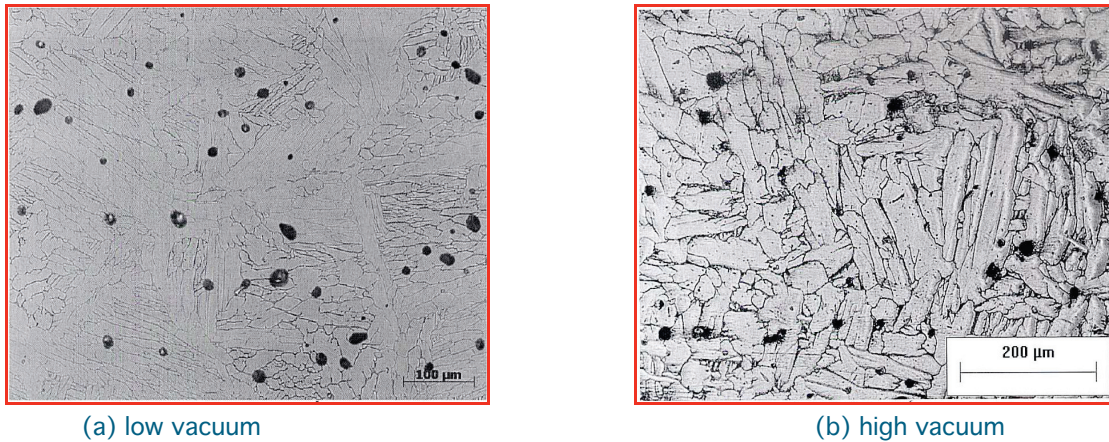


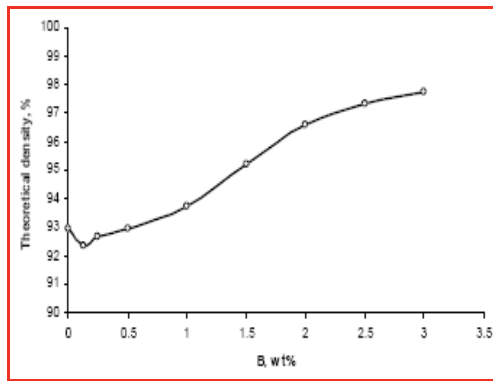
Figure 7. SEM images sintered Ti alloys in two vacuum levels.

Table 7. Mechanical properties of Ti-Fe-Zr alloys

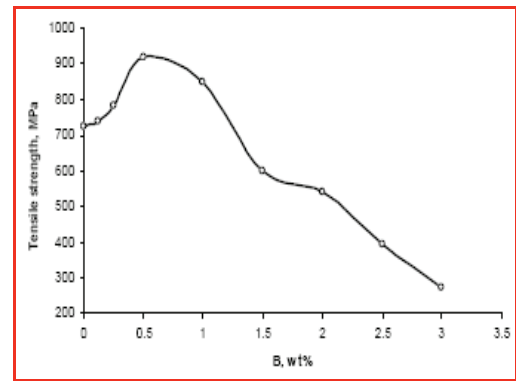
Powder	Composition	Density (%)	Strength (MPa)	Elongation (%)	Vacuum (mtorr)
HDH	Pure Ti	91.8	643	3.13	10
	5Fe-2.5Zr	95.0	1025	3.54	
	5Fe-5Zr	94.0	1127	2.50	
Sponge	Pure Ti	94.8	524	4.52	0.3
	5Fe-2.5Zr	96.6	983	3.91	
	5Fe-5Zr	96.4	1067	3.20	

## Evaluation of Boride Ti Alloys

As we proposed, the boride Ti alloy is one of the possible candidates for structural materials. We investigated the sintering behavior, the microstructure, and the mechanical properties of Ti-5Fe alloy with boron additions for structural applications, as shown in Figures 8 and 9. Samples were produced by the mixing of initial pure metallic powders followed by uniaxial pressing with subsequent densification by sintering 1200 °C and 1300 °C in vacuum. SEM was used to study the characterization of the microstructure of the sintered samples. Hardness and tensile tests were performed for different samples. The results show that with increases of boron, the theoretical density, the tensile strength, and the hardness all increase, but the ductility decreases.



(a) density



(b) tensile strength

Figure 8. Sintering behavior and mechanical properties.

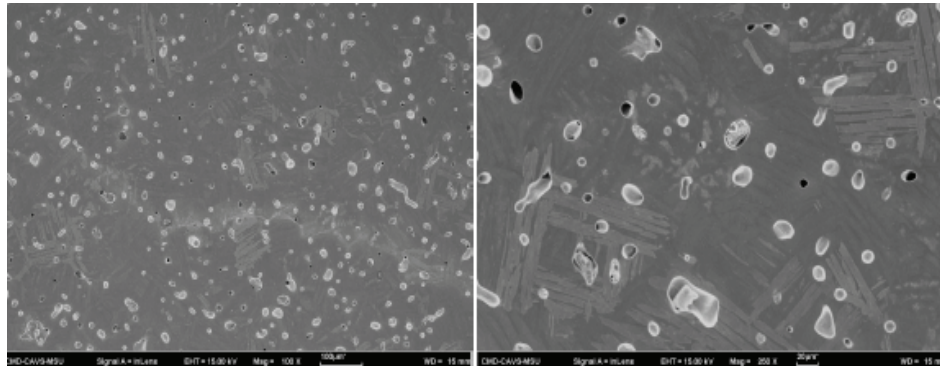


Figure 9. SEM images of Ti-5Fe-0.5CrB<sub>2</sub>.

## Powder Injection Molding (PIM) Experiment

New binder formulation was chosen for sponge and HDH Ti powder injection molding to avoid formation of TiC which is given as follows:

- 65 wt.% paraffin wax
- 25 wt.% low density polypropylene
- 9 wt.% Fusabond
- 1 wt% stearic acid
- 50 vol. % solid loading of -325 mesh Ti-HDH powder by determined by torque rheometer.

Initial trials on injection molding for three different compositions were conducted with the Ti alloy feedstock (Figure 10). After injection molding, the binder components were extracted by two methods. As for the lower molecular weight components such as paraffin wax and stearic acid, the solvent debinding process was used in n-haptane. Figure 11 shows the weight loss with time for two different samples during solvent debinding. As for the high molecular weight binder components, the thermal debinding process was used in furnace. To determine the optimum thermal cycle of thermal debinding, TGA/DSC was used, as shown in Figure 12.



Figure 10. Molding trial by Ti alloy feedstock.

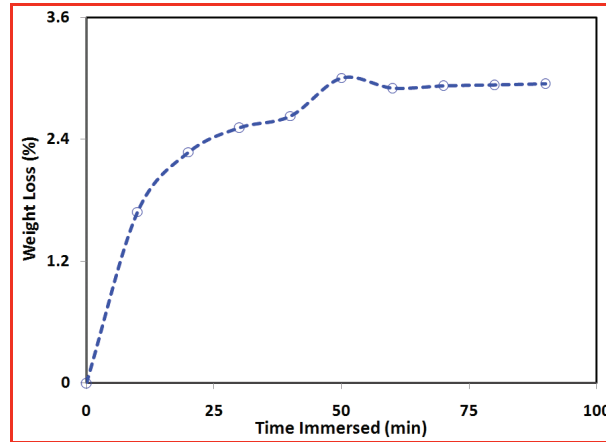


Figure 11. Plot of weight loss versus time during solvent debinding.

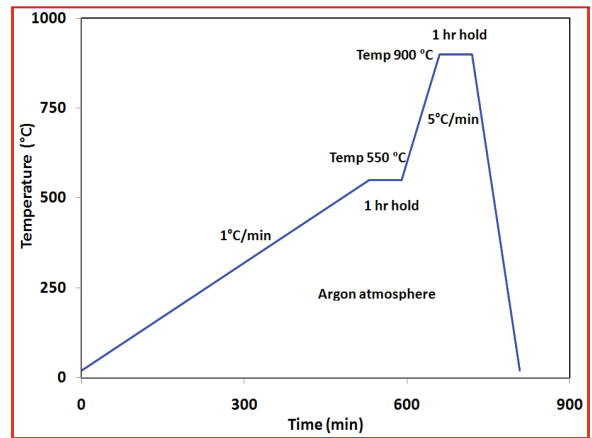
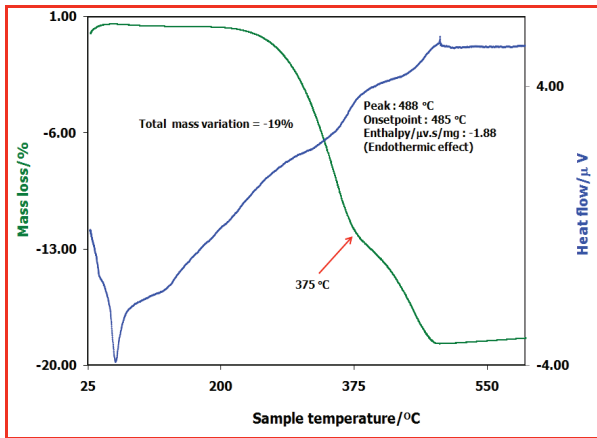


Figure 12. Thermal debinding: (a) plot of weight loss and heat flow versus temperature by TGA/DSC and (b) optimum thermal debinding cycle.

After removing all binder components, the sintering process was used to produce the final parts. Two sintering temperatures (1275 and 1300 °C) and holding time (1 & 2 hr) were chosen in this study. The vacuum furnace used in this effort was an MRF 1 cubic foot furnace that was equipped with 4 sided heating. The hot zone and heating elements were all refractory metals. The furnace achieved vacuum level of  $5 \times 10^{-5}$  torr. Figure 13 shows the used sintering cycle in this research and Figure 14 shows the appearance of both green and sintered samples. The maximum mechanical properties achieved under these conditions are shown in Table 8.

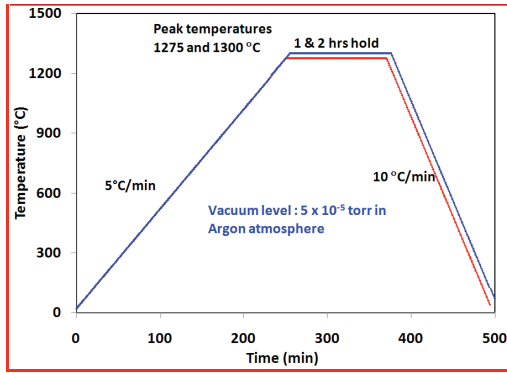


Figure 13. Sintering cycle for producing the final part.

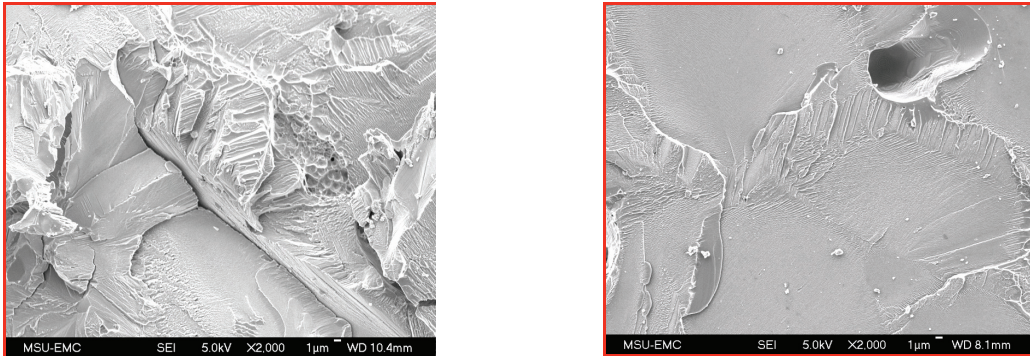


Figure 14. Green and sintered PIM parts arranged alternately.

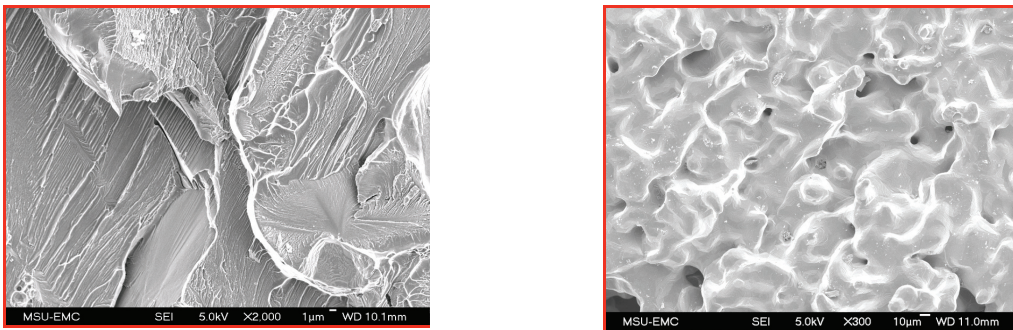
Table 8. Mechanical properties of sintered PIM Ti parts

Alloy	Sintering Temp (°C)	Hold (hr)	$\rho_{th}$ (g cm <sup>-3</sup> )	Green Sample		Sintered Sample				
				$\rho_g$ (g cm <sup>-3</sup> )	Relative Density (%)	$\rho_s$ (g cm <sup>-3</sup> )	Relative Density (%)	Hardness (HRB)	Elongation (%)	UTS (MPa)
Ti	1275	1	4.51	2.97	65.8	3.62	80.3	58.9	1.26	190
		2		3.03	67.2	3.92	86.8	77.2	1.87	539
	1300	1		2.97	65.8	3.88	86.0	64.2	0.99	580
		2		2.99	66.2	3.91	86.8	69.7	1.41	517
Ti-5Fe-2.5Zr	1275	1	4.64	3.16	68.2	4.01	86.5	72.9	0.84	459
		2		3.16	68.1	4.02	86.6	76.9	0.89	508
	1300	1		3.16	68.1	4.00	86.2	71.9	0.32	237
		2		3.17	68.2	4.18	90.0	81.5	2.08	512
Ti-5Fe-5Zr	1275	1	4.68	2.77	59.2	4.14	88.6	74.5	2.26	410
		2		2.87	61.4	4.27	91.2	75.7	0.94	530
	1300	1		2.77	59.2	4.15	88.7	74.2	1.14	548
		2		2.85	60.9	3.91	83.5	72.1	0.00	198

As far as UTS values are concerned, the value obtained for PIM Ti alloys are lower than the parts produced by die compaction method. The scanning electron micrographs of the sintered parts presented in Figure 15 illustrate the existence of pores, brittle fracture regions and other defects regions, caused for poor densification and sintering response. Therefore, further research focusing on optimizing the sintering conditions is essential for the improvement of UTS values.



(a) Ti-5Fe-5Zr alloy

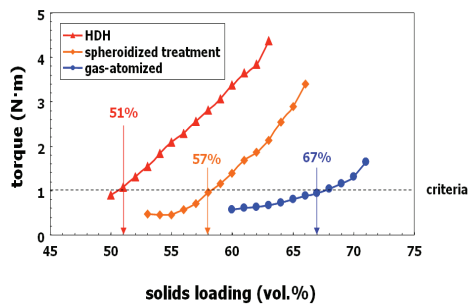


(b) Ti-5Fe-2.5Zr alloy

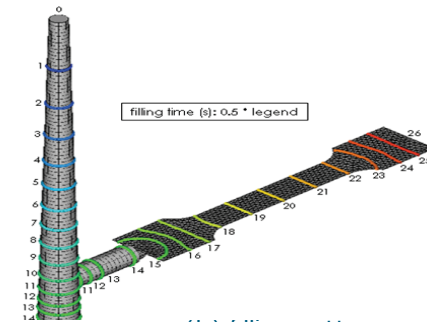
Figure 15. SEM images of sintered PIM Ti alloys.

## Modeling and Simulation

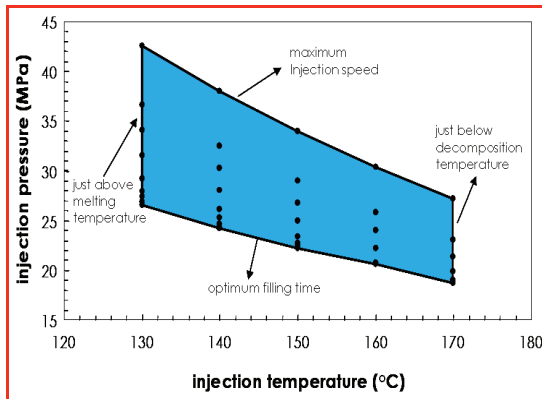
We first compared flow behavior of three different Ti powders: gas atomized, HDH, and spheroidized HDH Ti powders, as shown in Figure 16(a). We obtained the material properties from the literature of HDH Ti powder PIM for PIM simulation, using donated PIMsolver® (CetaTech Inc.). We selected the tensile specimen as the first geometry. We performed the first analysis simulation (Figure 16(b)), found possible processing windows (Figure 16(c)), and optimized the filling time for minimum injection pressure (Figure 16(d)).



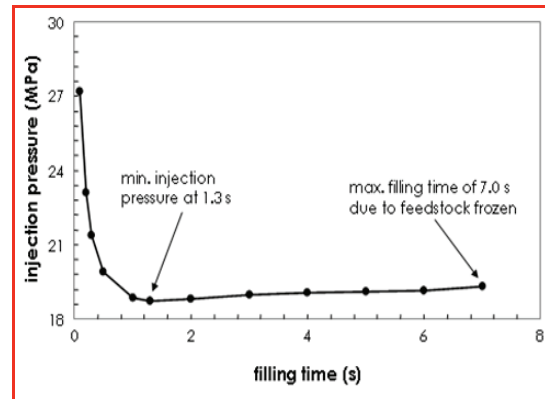
(a) torque vs. solid loading



(b) filling pattern



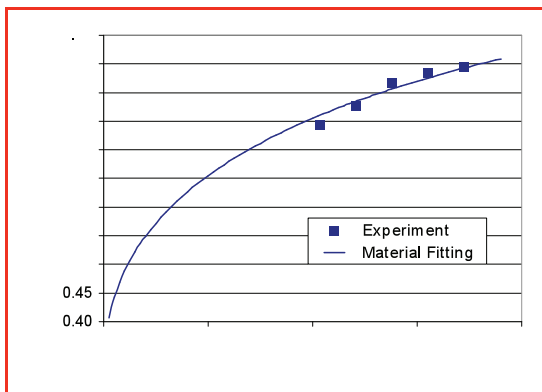
(c) processing window



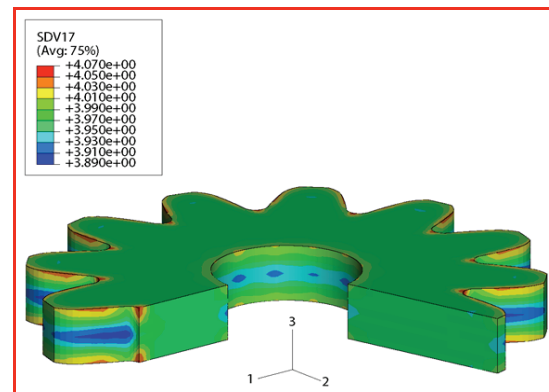
(d) optimum filling time

Figure 16. First trial of PIM simulation and optimization with HDH Ti powder.

**Die Compaction:** We obtained all material properties from a compressibility curve (Figure 17(a)) in the literature of commercial pure (CP) Ti powder for die compaction simulation using ABAQUS. We selected the gear as the first geometry. We performed the first analysis simulation (Figure 17(b)). We have the optimization algorithm for the loading schedule for uniform green compact density.



(a) compressibility curve



(b) density distribution after compaction

Figure 17. First trial of die compaction simulation with CP Ti powder.

**Sintering and HIPing:** We also have the capability to simulate sintering and HIPing processes. As for the HIPing, we obtained all material properties from the creep test with pressure and temperature dependency of Ti-6Al-4V powder, and we performed simulation for powder and can. In addition, we also have developed the algorithm to optimize can geometry in order to obtain the accurate final HIPed component dimension. However, we could not find any Ti powder or Ti alloy powder material properties for simulations for the sintering in the literature.

## Conclusions

---

During the project period, the following has been accomplished:

- Literature survey for low cost Ti powder, Ti alloys for automotive application with cost analysis, and their processing techniques.
- Design and evaluation of new Ti alloys, including boride Ti alloy.
- Experimentation of powder injection molding.
- Simulation tool development for powder injection molding, die compaction, sintering, and HIPing with some optimization.

## Presentations/Publications/Patents

---

### *Journal Publications:*

1. Park SJ, Wu Y, Heaney DF, Zou X, Gai G, and German RM. Rheological and thermal debinding behaviors in titanium powder injection molding. *Metallurgical and Materials Transactions A* 2009 Jan; 40(1): 215-22.
2. ElKadiri H, Wang L, Gulsoy HO, Suri P, Park SJ, Hammi Y, and German RM. Development of Ti based alloy: Design and experiment. *Journal of the Minerals, Metals and Materials Society (JOM)* 2009 May; 61(5): 60-6.

### *Conference Presentations:*

1. Gulsoy O, Suri P, El Kadiri H, Park SJ, Hammi Y, German RM, Peter W, and Blue G. Microstructure and Mechanical Properties of Sponge Ti and Its Alloy Powders with Various Powder Metallurgical Processes. TMS 2008; 2008 Mar 9-13; New Orleans, LA.
2. Gulsoy O, Suri P, Antonyraj A, Park SJ, German RM, ElKadiri H, Peter WH, and Blue C. Investigations on novel titanium alloys for structural applications. PM 2008; 2008 Jun 8-12; Washington, DC.
3. Gulsoy HO, Suri P, Park SJ, and German RM. Effect of boron additions on microstructural and mechanical properties of Ti-5Fe alloy for structural applications. 5th International PM Conference; 2008 Oct 8-12; Ankara, Turkey.
4. Gulsoy O, Suri P, Antonyraj A, Park SJ, German RM, and Wang P. Development of Powder Injection Molding Process for Sponge Ti Alloy. TMS 2009; 2009 Feb 15-19; San Francisco, CA.
5. Gulsoy O, Suri P, Antonyraj A, Park SJ, German RM, and Wang P. Development of Powder Injection Molding Process for Sponge Ti Alloy. PIM 2009; 2009 Mar 2-5; Orlando, FL.

### *Patents (in preparation):*

1. Three Ti alloy compositions

## References

---

- [1]. F.H. Froes and M.A. Imam, "Cost Affordable Developments in Titanium Technology and Applications," *Affordable Titanium III*, ed. M.A. Imam, F.H. Froes, and K.F. Dring (Zurich: Trans Tech Publications, 2010), pp. 1-12.

## C. Powder-Metal Performance Modeling of Automotive Components

---

Principal Investigator: Mark F. Horstemeyer (Paul T. Wang, Youssef Hammi)  
Chair Professor in Solid Mechanics at the Center for Advanced Vehicular Systems  
Professor in Mechanical Engineering  
Mississippi State University  
206 Carpenter Bldg., P.O. Box ME  
Mississippi State, MS 39762  
(662) 325-7308; e-mail: mfhorst@me.msstate.edu

Paulo Rosa, Materials Engineering Lead - Powertrain  
Chrysler LLC  
800 Chrysler Drive, CIMS 484-01-07  
Auburn Hills, MI 48326  
(248) 576-3197; e-mail: pr31@chrysler.com

Shekhar G. Wakade, Technical Specialist Materials Engineering  
GM Powertrain  
823 Joslyn Ave.  
Pontiac, MI 48340  
(248) 568-1143; e-mail: shekhar.g.wakade@gm.com

Glen Weber, Technical Specialist Engine Metals  
Ford Motor Company  
Building #1, Cube 12A037  
Dearborn, MI  
(313) 322-0175; e-mail: gweber@ford.com

Russell A. Chernenkoff, (retired from Ford Motor Company)  
Metaldyne LLC.  
Metaldyne Headquarters  
47659 Halyard Drive  
Plymouth, MI 48170  
(734) 582-6227; e-mail: russellchernenkoff@metaldyne.com

Technical Program Administrator: Eric McCarty  
Materials Technologies Consulting, LLC  
5609 Hummingbird Lane  
Clarkston, Michigan 48346  
(248) 520-3009; e-mail: eric.mccarty@sbcglobal.net

Technology Area Development Manager: William Joost  
(202) 287-6020; e-mail: william.joost@ee.doe.gov

Field Project Officer: Magda A. Rivera  
(304) 285-1359; email: magda.rivera@netl.doe.gov

Contractor: U.S. Automotive Materials Partnership (AMD 410)  
Contract No.: FC-26-02OR22910

## Objective

---

Our objective is to develop and experimentally validate math-based models for powder metallurgy component design and performance prediction. We will extend an existing Automotive Materials Partnership (USAMP) microstructure-property model from casting to powder metallurgy (PM) for practical application in low strain rate (design and durability) and high strain rate (toughness driven impact strength) environments. We will use this model to evaluate and optimize an automotive component design (main bearing cap) as affected by materials (ferrous and non-ferrous) and manufacturing processes (compaction and sintering). We will implement this model into various software platforms (such as ABAQUS). This model will be robust enough to facilitate the insertion of various lightweight materials (such as aluminum and titanium) for future component applications.

## Approach

---

- *TASK 1:* Determine current PM standards publications, component design guidelines, manufacturing, and evaluation methodologies. Provide a selection of metal powders that can satisfy design performance requirements, component design guidelines, and manufacturing and testing specifications across industry participants.
- *TASK 2:* Evaluate and develop numerical modeling techniques to predict mechanical properties throughout PM component sections. The transition of current materials/design requirements to advanced structural PM components has created a need to predict the properties of components in all sections of design. In addition, design processes should consider the least cost, lowest mass product designs and reduced development lead-time. We will extend an existing math-based framework with the abilities to predict PM component structures and properties accurately throughout the compaction and sintering processes (section size, density variation, dimensional tolerances, potential for cracking), and with the input of alloys and process parameters (machine functions, tool and powder temperatures, friction and pressure). We will capture the history of a PM part through its pressing, sintering, and life-cycle performance using the developed multiscale methodology.
- *TASK 3:* Develop component and vehicle level testing to validate durability, quality control and performance of PM parts. We will determine quality control process factors (powder properties, press settings, tooling design, and furnace conditions) for PM parts production in terms of their impact on process variations and quality improvement. We will use optimization and statistical techniques to help determine the main factors affecting the final component. We will perform validation experiments considering actual boundary conditions from real processes to fracture of the components.
- *TASK 4:* Manage and report program activities. We will incorporate monthly teleconferences, have two technical review sessions per year and have intermittent meetings throughout the year to report progress and discuss issues. Proper execution of this task will greatly enhance the visibility and the value of this program. Reports generated from this program will follow the guidelines suggested by DOE and the United States Council for Automotive Research (USCAR).
- *TASK 5:* Perform Technology/Commercial transfer throughout the product value chain. To date, there exists limited accountability for major R&D/technical institutions to foster the infrastructure to support large-scale applications of PM components. If the auto industry wishes to take advantage of PM's potential weight and cost reduction opportunities, they must nurture PM development through programs sponsored and directed by USCAR. The project team will request the professional support of societies to publish notices of meetings and project information, as released by the project team.

## Milestones, Metrics and Accomplishments

---

### *TASK 1 – COMPLETED 2006*

### *TASK 2 – COMPLETED 2008*

- Compaction, Sintering and Performance models complete.
- Performed sintering analysis of the main bearing cap for the FC-0205 and 205Q powders using experimental data
- Correlated the FC-0205 and 205Q sintering data with the model
- Performed sintering analysis for an aluminum alloy using literature data

### *TASK 3 – COMPLETED 2009*

- Validated the sintering simulation, compaction model and fatigue model with results with the experimental results on the main bearing cap.
- Used the model to optimize the compaction process for a main bearing cap.
- Performed optimization simulations of the main bearing cap.

### *TASK 4 - INCOMPLETE*

- Submitted two conference papers for MPIF-PM2009.
- Final Report expected in November, 2009

### *TASK 5 - COMPLETE 2008*

- Technology transfer - OEM, supplier and Mississippi State University meeting to demonstrate compaction and sintering models.
- Submitted user guide for the math-based model developed in this program for PM component design and performance prediction.

### *2009 PROGRESS*

The compaction, sintering and performance models were completed in 2008. The work in 2009 verified the models by fatigue testing production main bearing caps and comparing the results against model predictions. This work was completed in June, 2006 and the remaining time has been used to write the Final Report, which was completed in November, 2009 and is pending approval.

## Introduction

---

The objective of this project is to develop and experimentally validate math-based models for PM component design and performance prediction.

During the last six months, the remaining experiments were completed for characterization and validation of the constitutive equations for sintering. We performed dilatometer experiments on FC-0205 and FC-0208 powders to study the shrinkage of these powders during sintering.

Using the material parameters from the dilatometer and image analysis experiments, we described the evolution of the porosity or density during the sintering process using constitutive equations. The sintering model was validated by applying it to a steel main bearing cap (MBC), where the sintering model input included compaction model density and stress distribution results from a previous developed constitutive model.

Math-based models developed by the MSU/CAVS team have considered both the compaction and sintering processes. Through further numerical analysis the output of the compaction model was optimized for one or more output parameters, e.g. least density variation, lowest mass, minimal part thickness.

## Sintering Modeling

Sintering is probably the most complicated of the PM process. During sintering, the strength of the compacted part is increased due to diffusion and bonding between particles. Therefore successful modeling of the sintering process must capture the heat transfer and phase transformations during sintering, as well as accurately predict the shape change during densification. By describing the evolution of the porosity or density during the sintering process using constitutive equations with known material parameters, we can gain a better understanding of the structure-property changes during the process and better predict the behavior of the powder during sintering.

## Master Sintering Curve

The master sintering curve (MSC) was derived from densification data obtained over a range of heating rates or sintering temperatures. When the proper activation energy is chosen, all the data converge to a single “master sintering” curve. The developed MSC is therefore unique for a given powder, green microstructure and green density. Any changes to the particle size distribution, average particle size, initial pore-size distribution, and particle packing properties will modify the green microstructure and ultimately the constructed MSC. Under these assumptions and after rearrangement of the combined stage sintering equation, the master sintering curve equation  $\Theta(\rho)$  was developed from the following equation [1-3]:

$$\Theta(\rho) \equiv \Theta[t, T(t)] = \int_{t_0}^t \frac{1}{T} \exp\left(-\frac{Q_b}{RT}\right) dt \cdot \quad (1)$$

The apparent activation energy  $Q_b$  for sintering defines the master sintering curve and was obtained using shrinkage data from either isothermal or constant-heating rate experiments. By comparing the activation energy derived from experimental data to published values for activation energies associated with specific diffusional paths, i.e., volume, surface, or grain boundary diffusion, we identified the primary diffusional mechanisms responsible for sintering. The apparent sintering activation energy was obtained by minimizing the normalized dimensionless mean residual square, defined as

$$\text{Mean residual square} = \frac{1}{\rho_f - \rho_0} \int_{\rho_0}^{\rho_f} \frac{\sum_i^N [(\Theta_i / \Theta_{avg}) - 1]^2}{N} d\rho \quad (2)$$

where  $N$  is the number of experimental dilatometry tests,  $\Theta_{avg}$  is the average of all  $\Theta_i$  over  $N$ ,  $\rho_0$  is the initial (green) density and  $\rho_f$  is the final (sintered) density.

Figure 1 has the flowchart detailing the overall algorithm used to convert dilatometer data into the final sigmoid curve function describing grain growth plot and the master sintering curve.

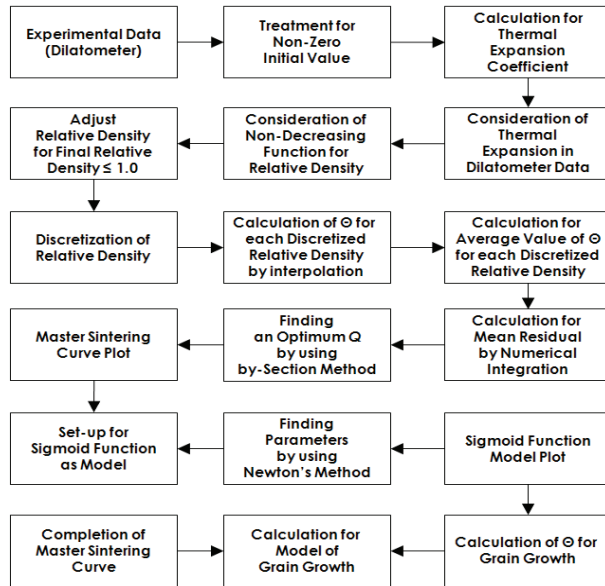


Figure 1. Overall algorithm for construction of master sintering curve.

## Densification

A comparison of the dimensional change from the dilatometer experiments for FC-0205 and FC-0208 compacts heated at 10°C/min; along with the corresponding temperature cycle is shown in Figure 2. Changes in the rate of shrinkage were linked to microstructural evolution and thermophysical events or chemical reactions [24]. As expected both powders have similarly shaped dilatometry profiles with dissimilar magnitudes of dimensional change due to the effects of the alloying additions. The FC-0205 compact presents more dimensional change than the FC-0208 after sintering due to the difference in alloy composition and powder size. The extra 0.3 % of carbon in the FC-0208 reduces the swelling caused by the molten copper. And the fine copper particles can cause more volumetric change than coarse particles. The particle size of copper was not investigated in this study. After sintering the Fe-Cu-C system had improved hardness and strength due to the precipitation hardening by the copper and the strengthening by the carbon.

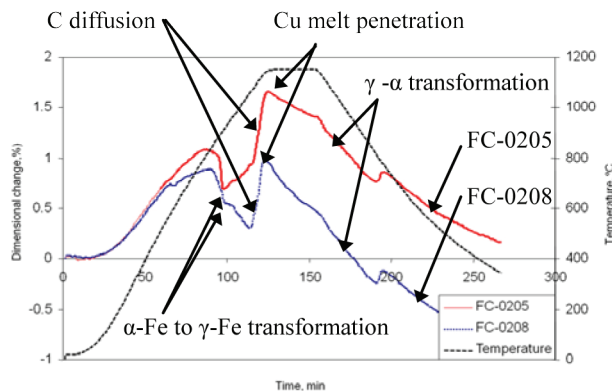


Figure 2. Dilatometer curves of dimensional change for the FC-0205 and FC-0208 with a heating rate of 10°C/min.

# Construction of Master Sintering Curve

The MSC is generated from the measured densities as a function of  $\theta$ , using isothermal or non-isothermal methods. The dilatometer results in Figure 3 compare the relative density of FC-0205 samples having initial relative densities of 0.612 and 0.81, and heated at 2°C/min, 5°C/min, and 10°C/min. From the dilatometer experiments at various constant heating rates, the final densities were measured, and the density at previous times was computed from the linear shrinkage data. The results indicated that the sintered density increased as the heating rate decreased.

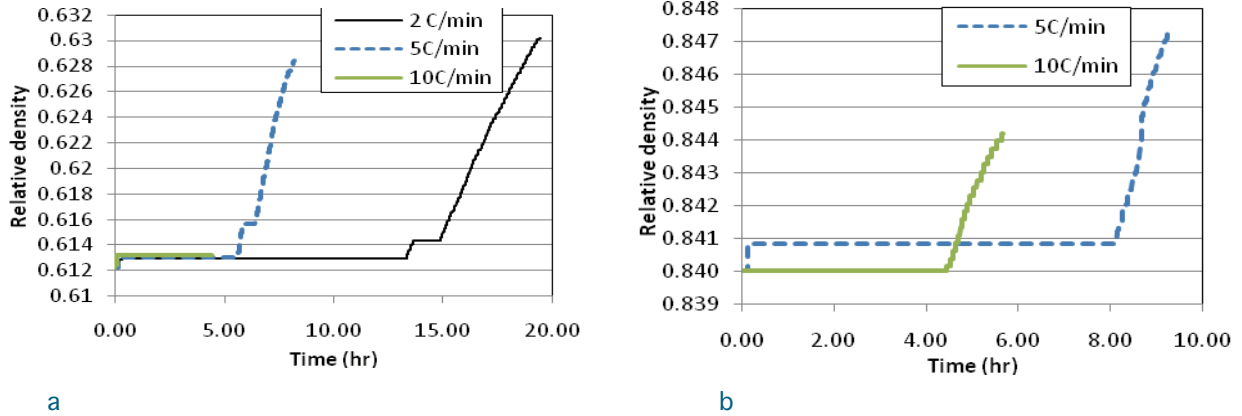


Figure 3. Density as function of time for different constant heating rate for (a) 0.61 and (b) 0.84 initial relative density.

Using Eq. (1), the value of  $\theta$  was computed for each data point, using an assumed value of the activation energy. As shown in Figure 4, the mean residual for different given values of activation energy  $Q$  was determined from Eq. (2) and plotted in order to graphically find the optimal activation energy  $Q$ . The number of values of activation energy  $Q$  was increased to refine and increase the accuracy of the method. From the activation energy  $Q$ , the sigmoid function was determined. As shown in Figure 5, by plotting density versus  $\log(\theta)$ , the MSC was obtained of the FC-0205 powder.

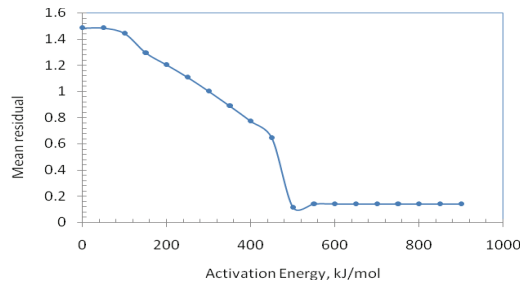


Figure 4. Mean Residual for determining the activation  $Q_b$

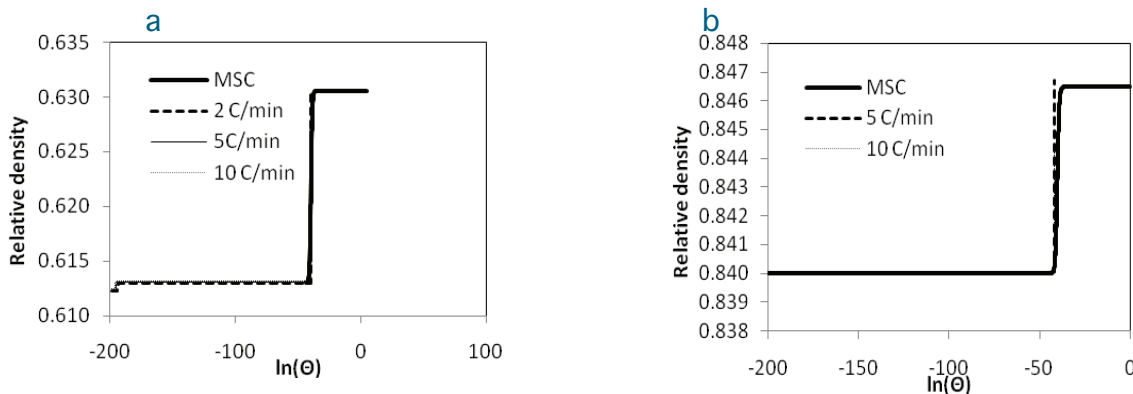


Figure 5. Calculated Master Sintering Curve for the FC-0205 powder with (a) 0.61 and (b) 0.84 initial relative density.

## Sintering Model Implementation

The dimensional changes from the dilatometer experiments, as well as the results from the microstructure analysis, were used to calibrate sintering parameters and to verify the predictive capability of the model. The sintering model was implemented in the user material subroutine UMAT using an implicit stress integration algorithm [4]. The sintering mechanism was also described as a diffusional creep behavior, therefore a subroutine identical to the user subroutine CREEP of ABAQUS was called inside UMAT. Although this creep subroutine can be called independently by ABAQUS, it was implemented in conjunction with UMAT to give to the user the freedom to increase the complexity of the sintering model. Several solution-dependent state variables (SDV) were defined and stored as part of the material solution. And while certain variables were needed for solving the next increment, other variables, such as sintering stress, bulk and shear viscosities, were used for post-processing only.

To calibrate the FC-0205 sintering material parameters, a comparison between the dilatometer experiments and the numerical analysis on axial shrinkage was performed. The numerical analysis was performed using axisymmetric elements (CAX4). Because the FC-0205 powder is mainly composed of iron, we assumed the linear thermal expansion coefficient of the FC-0205 powder compact is the same as that of pure iron and is defined as temperature-dependent in the numerical analysis. The material conductivity of the metal powder compact is  $10.0 \text{ W m}^{-1} \text{ K}^{-1}$ .

Using the sintering material parameters obtained from the experimental results, the numerical analysis was performed. Figure 6 shows good agreement between the numerical and experimental axial shrinkage of FC-0205 during sintering. Specifically, the simulation results indicated a transition point when the sintering stress (around  $1100^\circ\text{C}$ ) began to dominate and thermal expansion effects were less pronounced. However, the axial shrinkage from the simulation did not capture the microstructural changes and phase transformations during sintering as observed in the experiments. These changes in the slope of the shrinkage response were due to the solid state diffusion of the iron-copper-carbon system in the early stage of sintering and liquid state sintering once the copper reached the melting temperature, as well as from the  $\alpha$ - $\gamma$  phase transformations as shown in Figure 2. The mean grain size in the MBC at the end of the sintering process was  $15 \mu\text{m}$ , as measured from the image analysis measurement of different sections of the MBC. In the FEA results, the final mean grain size was  $17.5 \mu\text{m}$ .

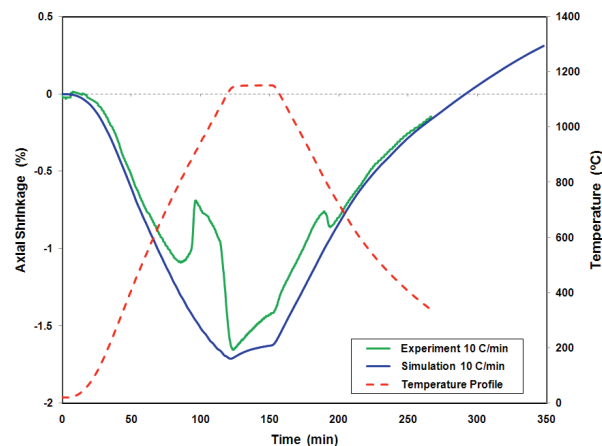


Figure 6. Comparison of axial shrinkage and temperature profile between the dilatometer experiments and the FEM model prediction for FC-0205 powder compacts (0.60 relative density) sintered in Nitrogen at  $10^\circ\text{C}/\text{min}$  to  $1120^\circ\text{C}$  with 30-minute hold time.



# Optimization Study

---

## *Finite Element Model*

Because the MBC is an automotive component, the main objectives in optimizing the current steel design were to reduce weight (and therefore cost), to increase fatigue life and to improve the life cycle performance of the component. To capture the life cycle performance in design, one must understand the materials processing history first. The finite element analysis included the compaction of the powder material, springback (ejection) analysis and the performance analysis. Internal state variables were used in the material model to reflect the dislocation density, pore growth, and pore coalescence from the PM microstructural features under different temperatures, strain rates, and deformation paths.

Using the calibrated microstructure-property material model and the microstructural heterogeneities as simulated by the compaction and sintering models, the performance model was used in a finite element analysis to predict failure. The model for the monotonic test consisted of the MBC as a deformable body with two rods going through each end of the bearing cap. The rods were meshed as a rigid body with R3D4 rigid elements, while the bearing cap was meshed using C3D8R continuum brick elements. Boundary conditions were applied to the rods, with loading applied to one rod while the other rod remained fixed. The porosity distribution of the MBC from the compaction computational results were mapped into the springback model, whose resulting porosity distribution was then transferred to the performance model, which predicted the failure location.

The fatigue analysis followed the same procedure of transferring the density distribution from the compaction analysis to the springback analysis and then to the performance analysis and finally to the fatigue analysis. In this work a MultiStage Fatigue (MSF) model comprising an incubation stage, microstructurally small crack (MSC) stage, and a long crack stage was used to predict the fatigue failure. The input microstructural features and the stress, strain, and damage states came from the microstructure-property material model used in the finite element analysis. Each component of the fatigue fixture was assumed elastic (Young's modulus  $E=200,000$  MPa and Poisson's ratio  $\nu=0.33$ ) except the shaft, which was assumed rigid for simplification purpose. The shaft was meshed as a rigid body with R3D4 rigid elements, while the other components of the fatigue fixture were assumed elastic and were modeled with C3D8R continuum brick elements. Once the MSF model received the inputs from the performance model, the final fatigue failure locations and number of cycles to failure were predicted. Under the maximum shaft loading, the stresses throughout the MBC were within the elastic domain, so high cycle fatigue was the main issue under fatigue.

## *Optimization*

The optimization problem was based on the compaction and performance ISV models of the MBC. To minimize the number of simulations needed in order to obtain meaningful conclusions regarding possible design modifications, we used Design of Experiments (DOE) for the numerical optimization analysis. In our case we examined the effects of various dimensional changes on the density distribution and performance of the MBC using the validated compaction and performance ISV models that will be published later. In the current study we used the Taguchi orthogonal array for optimizing the MBC. The Taguchi method<sup>7</sup> dramatically reduced number of design points required to find the effective parametric factors has been successfully used in crashworthiness optimizations of a 1996 Dodge Neon [8].

The Taguchi optimization method gives us the optimum design based upon the parameters generated within the upper and lower limits of the design variables. Parameters, such as the mass and volume of the bearing cap were obtained from the finite element analysis of the bearing cap. Due to constraints of the crank and bolts going through the bearing cap, four design variables, including three radii and the MBC thickness, were selected as shown in Figure

9. Based upon the design variables and their minimum and maximum values, the design matrix consisted of nine different MBC designs that were simulated with the parameters as shown in the Table 1, which also includes the FEA responses for the original MBC design.

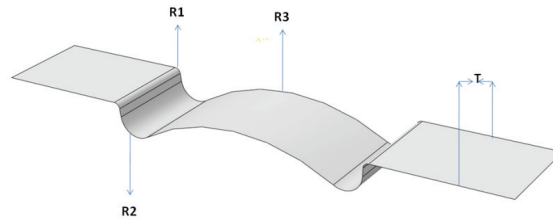


Figure 9. The top view of bearing cap with design variables (R1,R2,R3, and T) for the optimization.

Table 1: Design matrix and responses obtained from FE simulations

Case	Design Variables (mm)				FEA Responses	
	R1	R2	R3	T	f <sub>1</sub> (x) (strain)	f <sub>2</sub> (x) (density)
1	1	3	47	20	0.000877	6.905375
2	1	4.5	48.675	21	0.009883	6.874384
3	1	6	50.35	22	0.009149	6.84232
4	1.25	3	48.675	22	0.006734	6.89125
5	1.25	4.5	50.35	20	-2.11E-05	6.852684
6	1.25	6	47	21	0.005473	6.853793
7	1.5	3	50.35	21	-0.00295	6.875455
8	1.5	4.5	47	22	0.009365	6.8768
9	1.5	6	48.675	20	0.008857	6.829785

Before optimization, we developed the appropriate metamodels for the objective functions  $f_1(x)$ ,  $f_2(x)$  using a second-order polynomial Response Surface Methodology (RSM) in the form

$$f'(x) = \beta_0 + \sum_{i=1}^m \beta_i x_i + \sum_{i=1}^m \beta_{ii} x_i^2 + \sum_{i=1}^{m-1} \sum_{j=i+1}^m \beta_{ij} x_i x_j \quad (3)$$

where  $f'(x)$  is the approximate value of the true objective function  $f(x)$ ,  $m$  is the total number of design variables,  $x_i$  is the  $i^{\text{th}}$  design variable, and the  $\beta$ 's are unknown coefficients to be solved using the method of least squares. The multi-objective optimization problem was solved using the object-oriented multidisciplinary optimization system developed at the Center for Advanced Vehicular Systems, Mississippi State University [9].

### Optimization Results

The main goal of optimization for the MBC was to increase the overall strength of the component without negatively affecting its performance as compared to the current design. Using the Taguchi optimization method discussed previously, we obtained an optimum solution for the bearing cap parameters, as provided in Table 2. The revised dimensions resulted in a reduced material volume of 4.5% and a decreased weight of 3.8%.

Table 2: Comparison of initial and optimal designs

Item	Before optimization	After optimization	% Change
R1 (mm)	1.5	1.31	-12.7
R2 (mm)	5	6	20
R3 (mm)	50.35	50.35	0
T (mm)	22	21.232	-3.5
Mass (g)	725.4	697.6	-3.8
Volume (cc)	108.6	103.65	-4.5
Cycles to Failure (23,000 lbs)	7,554,681	8,307,369	9.5
Performance (displacement-mm)	1.63	1.71	5

Furthermore, the optimum design with modified design variables was simulated in ABAQUS for comparing its performance with the existing bearing cap design. The finite element simulation followed the same procedure as described earlier for obtaining the parameters for optimization. The performance for the optimum design and the previous design was compared and is shown in Figure 10.

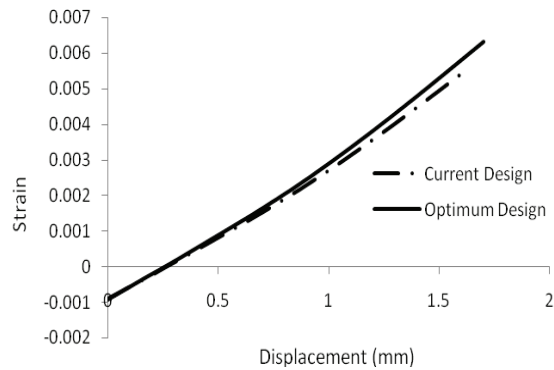


Figure 10. Comparison of the performance of the optimized MBC design and the current MBC design.

As shown in Table 2, the results of the optimization study also revealed that the modified design showed improved performance and an increase in fatigue life as compared with the current design. Figure 10 reveals that the optimum design gave better performance than the existing design by admitting more strain. The finite element analysis predicted a crack initiated after 1.71 mm of displacement in the optimum design, whereas the crack initiated after 1.63 mm displacement in the current design. Hence, as indicated in Table 3, the optimum design resulted in a 5% increase in performance as compared to the current design. Table 3 compares the fatigue life of the current design to that of the optimized design. The optimized design resulted in a “pass” at 21,000 lbs. of shaft loading compared to the current design which indicated a “crack” at the same loading. Thus, the optimum design resulted in a 9.5% increase in fatigue life. The optimization results obtained in this study are empirical and have not been validated.

Table 3. Cycles to failure for (a) the Current Design and (b) the Optimized Design.

Fatigue	Shaft loading (lbs)			
Life	20,000	21,000	22,000	23,000
Ntotal				
Failure	PASS	CRACK	FAIL	FAIL

(a)

Fatigue	Shaft loading (lbs)			
Life	20,000	21,000	22,000	23,000
Ntotal				
Failure	PASS	PASS	FAIL	FAIL

(b)

## Conclusions

---

We performed dilatometer experiments to construct master sintering curves relating sintered density to the work of sintering for FC-0205 and FC-0208 PM systems. Compared to the typical sintering behavior of other powder metals, the observed shrinkage in the FC-0205 and FC-0208 materials was very small, resulting in an overall dimensional change of only 0.2%. From the material parameters determined from the experiments, we described the evolution of the porosity or density during the sintering process using constitutive equations. A good agreement was obtained between the numerical and experimental axial shrinkage results of FC-0205 during sintering. The sintering model was validated by applying it to a steel MBC. The overall shrinkage in the model was approximately 0.2-0.3%, which compares favorably with measured density values of the MBC.

We employed the Taguchi optimization method to the MBC to reduce the weight, to increase fatigue life and to improve its performance. To capture the porosity distribution of the MBC from the compaction simulation, the computational results were mapped into the springback model, whose resulting porosity distribution was then transferred to the performance model. The resulting optimum MBC resulted in reduced material volume of 4.5% and decreased weight of 3.8%, while increasing the monotonic strength by 5%, and the fatigue life by 9.5%.

## Presentations/Publications/Patents

---

Stone, T.W., Hammi, Y., Carino, R.L., Horstemeyer, M.F., 2009, "Modeling for Powder Metallurgy Component Design and Performance Prediction," PowderMet 2009 Conference, Las Vegas, NV, June 28-July 1.

Stone, T.W., Sanderow, H., Grewal, H., Hammi, Y., Allison, P., Solanki, K., Horstemeyer, M.F., 2009, "Process Modeling: Use of Uncertainty, Sensitivity and Optimization Techniques for Improved Understanding of Compaction Model Outputs," PowderMet 2009 Conference, Las Vegas, NV, June 28-July 1.

## Acknowledgements

---

The authors would like to acknowledge funding from the Center for Advanced Vehicular Systems at Mississippi State University and from USAMP Automotive Metals Division (AMD) 410.

## References

---

1. H. Su and D.L. Johnson, "Master Sintering Curve: A Practical Approach to Sintering," J. Amer. Cer. Soc., 1996, 79 (12), pp. 3211-3217.
2. D.L. Johnson and H. Su, "The Master Sintering Curve", Advances in Powder Metallurgy and Particulate Materials, 1997, 2, pp. 14.115-14.121.
3. D.C. Blaine, S.J. Park, P. Suri, and R.M. German, "Application of Work-of-Sintering Concepts in Powder Metals," Metall Mater Trans A, 2006, 37A (9), pp. 2827-2835.
4. Govindarajan, R.M., and Aravas, N., "Deformation processing of metal powders: Part II – Hot isostatic pressing", Int. J. Mech Sci., 1994, 36 (4), pp. 359–372.
5. "MPIF Standard 42: Method for Determination of Density of Compacted or Sintered Powder Metallurgy Products", Standard Test Methods for Metal Powders and Powder Metallurgy Products, Metal Powders Industries Federation, Princeton, NJ, 2007, pp. 59-62.
6. T.W. Stone, L. Tucker, T.N. Williams, Y. Hammi, H. El Kadiri, M.F. Horstemeyer, "Comparison of Density Measurement Techniques for Large P/M Components," Proceedings of the 2008 World Congress on Powder Metallurgy and Particulate Materials, MPIF, Princeton, NJ, 2008, pp. 11.84-11-96.
7. Taguchi, G., System of Experimental Design. UNIPUB Kraus International Publications, New York, 1987.
8. Fang, H., Solanki, K.N., Horstemeyer, M., Numerical simulations of multiple vehicle crashes and multidisciplinary crashworthiness optimization. International Journal of Crashworthiness, 2005, 10(2), 161-172.
9. Fang, H. and Horstemeyer, M.F. An integrated design optimization framework using object-oriented programming. In: Proceedings of the 10th AIAA/ISSMP multidisciplinary analysis and optimization conference. Albany, NY: 2004. Paper no. AIAA-2004-4499.